Received 29 October 2022; accepted 18 November 2022. Date of publication 24 November 2022; date of current version 8 December 2022.

Digital Object Identifier 10.1109/OJCOMS.2022.3224576

Paving the Way Toward Mobile IAB: Problems, Solutions and Challenges

VICTOR F. MONTEIRO[1], FRANCISCO RAFAEL M. LIMA[1] (Senior Member, IEEE), DARLAN C. MOREIRA[1], DIEGO A. SOUSA[1,2], TARCISIO F. MACIEL[1], BEHROOZ MAKKI[3] (Senior Member, IEEE), AND HANS HANNU[4]

[1]Wireless Telecommunications Research Group (GTEL), Federal University of Ceará, Fortaleza 60440-900, Brazil

[2]Federal Institute of Education, Science, and Technology of Ceará (IFCE), Paracuru 62680-000, Brazil

[3]Ericsson Research, 417 56 Gothenburg, Sweden

[4]Ericsson Research, 977 53 Luleå, Sweden

CORRESPONDING AUTHOR: V. F. MONTEIRO (e-mail: victor@gtel.ufc.br)

This work was supported in part by the Ericsson Research, Sweden; in part by the Ericsson Innovation Center, Brazil, under UFC.49 Technical Cooperation Contract Ericsson/UFC; and in part by the Coordenação de Aperfeiçoamento de Pessoal de Nível Superior (CAPES), Brazil, under Grant 001. The work of Francisco Rafael M. Lima was supported by FUNCAP (edital BPI) under Grant BP4-0172-00245.01.00/20. The work of Tarcisio F. Maciel was supported by CNPq under Grant 312471/2021-1.

ABSTRACT Deploying access and backhaul as wireless links, a.k.a. integrated access and backhaul (IAB), is envisioned as a viable approach to enable flexible and dense networks. Even further, mobile IAB (mIAB) is a candidate solution to enhance the connectivity of multiple user equipment (UE) moving together. In this context, different of other works from the literature, the present work overviews the basis for the deployment of mIAB by presenting: 1) the current status of IAB standardization in the fifth generation (5G) new radio (NR); 2) a new taxonomy for state-of-the-art works regarding fixed IAB and mIAB; 3) an extensive performance analysis of mIAB based on simulation results; and 4) open challenges and potential future prospects of mIAB. Specifically, the proposed taxonomy classifies IAB works according to different perspectives and categorizes mIAB works according to the type of mobile node. For each type of mobile node, the main studied topics are presented. Regarding the performance evaluation, we consider an urban macro scenario where mIAB nodes are deployed in buses in order to improve the passengers' connection. The results show that, compared to other network architectures, the deployment of mIAB nodes remarkably improves the passengers' throughput and latency in both downlink and uplink.

INDEX TERMS 5G standardization, 6G, backhaul, integrated access and backhaul (IAB), mobile IAB, mobility, moving cell.

I. INTRODUCTION

5G NETWORKS are being designed and deployed considering a dense deployment of small cells in order to simultaneously serve more UEs with higher throughput and lower delay [1]. However, building from scratch a completely new infrastructure is costly and takes time [2]. Deploying a wireless backhaul is then envisioned to be a technically viable approach to enable flexible and dense network deployments [3].

Wireless backhaul has already been considered in the past. However, on the one hand, it has been based on non-standardized solutions, deployed on millimeter wave (mmWave) band apart of the spectrum used for access links and mainly designed for point-to-point (PTP) communications with good networking planning and line of sight (LOS) connections, as in [4], [5], [6], [7]. On the other hand, in 5G, access and backhaul links can be deployed in mmWave band in 5G networks that are expected to be dense, possibly unplanned and with low height access points, which requires the support of non-line of sight (NLOS) backhaul. These 5G characteristics are the main reasons why academia and industry are now investigating a standardized solution

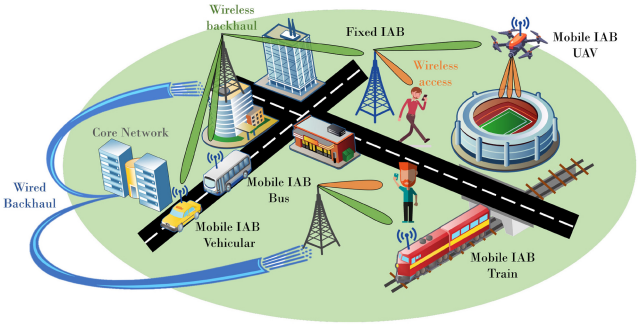

FIGURE 1. Overview scenario presenting examples of fixed IAB and mIAB use cases.

for joint access and backhaul fitting the 5G characteristics. The 3rd generation partnership project (3GPP), the organization in charge of standardizing 5G NR, has already started standardizing this new wireless backhaul under the term IAB.

IAB is promising and desirable due to its cost effectiveness,[1] fast deployment and easy maintenance [8]. Regarding the cost, the authors of [9] compared the deployment cost of three typical backhaul technologies, i.e., wireless, direct fiber and passive optical. They showed that a wireless backhaul is the most cost-effective among the three backhaul technologies. Another advantage is the support of larger bandwidth in NR without the need to proportionally densify the supporting wired transport network [3].

Thinking further, IAB also allows the deployment of mobile cells, called here mIAB cells, which should be available after 3GPP Release 18. The mIAB is expected to enhance the service of moving UEs improving connectivity to the network and to avoid signaling storms from simultaneous handover (HO) messages. Examples of mIAB applications are illustrated in Fig. 1, e.g., mIAB nodes deployed at trains, buses and unmanned aerial vehicles (UAVs).[2] In the examples presented in Fig. 1, the mIAB nodes are wirelessly served either by a base station (BS) which is connected by wire/fiber to the core network (CN) or even by a BS which is also wirelessly served by another BS wired-connected to the CN.

In terms of mobility, one can consider three distinct types of IAB nodes: fixed IAB nodes, nomadic IAB nodes and mIAB nodes. While fixed IAB nodes are always at the same position, allowing a system planning of long duration, nomadic IAB nodes adapt their location before the communication, remaining fixed during the communication. The main objective of nomadic IAB is to temporarily extend the coverage and serve out-vehicle UEs in a given area, e.g., disaster area, close to stadiums, etc. With mIAB, on the other hand, the mIAB node on top of, e.g., trains, buses, or trams, may communicate during the movement. As opposed to nomadic IAB, the main goal for mIAB is to serve the in-vehicle UEs. In this work, we concentrate on mIAB.

In this context, the present work aims at presenting an overview on the topic of mIAB and on the technologies enabling its deployment in 5G networks and beyond. At the time of writing of this work, as far as we know, [10] is the unique survey focused on IAB, while [11] is the most complete survey covering mobile cells.

The work in [10] focuses on fixed IAB. As opposed, we concentrate on the potentials and challenges of mIAB. Particularly, 1) we review and propose a taxonomy for works on mIAB which was not covered by [10]. Also, 2) different from [10], we present deep performance evaluations to verify the potential benefits of mIAB. Finally, while [10] presents a single taxonomy on fixed IAB, we present a different organization of the reviewed articles. More specifically, different from [10], we highlight that the works do not fit into a unique class of criteria as we classify the same work into different categories and under different perspectives.

Our work is different from [11] from various perspectives. Firstly, while the authors of [11] only focused on moving cells, we also address fixed IAB, which also uses a wireless backhaul. More specifically, we provide an overview of the architecture and protocols standardized by 3GPP to support IAB and, we present a taxonomy for fixed IAB works, which is the basis for mIAB in 5G and beyond 5G. Secondly, [11] only addresses land-based public transport vehicles such as trains, subways, buses, and vans, while we also address cars and UAVs. Finally, as [10], the survey in [11] does not present a detailed performance evaluation of mIAB and does not compare its performance with alternative technologies.

By presenting simulation results that take into account models, procedures and architectures standardized by 3GPP, we aim at comparing the performance of mIAB networks with current networks and at presenting future directions of research to improve its performance. Moreover, the results presented in the paper also provide interesting practical insights into the mIAB architecture, which adds to the existing research on this topic. Such results will be interesting for academical and industrial readers and may be useful in 3GPP discussions on mIAB. To the best of our knowledge, this is the only system-level performance evaluation of mIAB networks with realistic models showing the benefits and challenges of mIAB, in comparison with other deployment scenarios.

The present work is organized as follows. First, we present the basis of IAB in Sections II and III. More specifically, Section II presents current IAB aspects already standardized by 3GPP for 5G NR. Besides, Section III presents a literature review of fixed IAB. In this section, the works are classified following different criteria, such as: studied dimensions, system modeling assumptions/constraints, considered problem objectives and key performance indicators (KPIs), solution approaches and adopted mathematical tools. Furthermore, Section IV presents works related to mIAB. The works presented therein are firstly grouped based

1. The cost discussions and the details of the simulation parameter settings are not necessarily aligned with the Ericsson's points of interest.

2. UAV-based communication will not be part of the Release 18 discussions on mIAB.

on the existence or not of non-terrestrial links. Works of both groups, i.e., terrestrial and non-terrestrial, are classified according to the type of considered network nodes, e.g., train, bus, UAV, etc.. This is due to fact that works considering similar network nodes usually consider similar problems, e.g., UAV positioning, and take advantage of specific characteristics of each type of node, e.g., previously known mobile trajectory of buses. For each type of network node, we present the most recurrent topics and solutions presented in the literature. Moreover, Section V presents a performance evaluation of mIAB through computational simulations results. Extensive performance analysis is presented, including passengers' and pedestrians' throughput, latency and link quality in both downlink and uplink transmission directions. Results related to the wireless backhaul are also presented as well as the profile of links served by the IAB donors. Finally, Section VI summarizes the lessons learned and lists some open issues and future directions. Section VII presents the conclusions of this work.

II. IAB ON 3GPP

Wireless backhaul has been studied for years in the literature and the 3GPP has already taken some standardization actions on this matter in the context of long term evolution (LTE) Release 10 [12]. Although wireless backhaul is provided for BSs with the so called LTE relaying [13], the commercial interest on it was not as large as expected. The main limitations of LTE relaying are: 1) limited number of hops, i.e., only single hop is supported; 2) static parent to child architecture; 3) inflexible bandwidth partitioning between access and backhaul; and 4) limited available spectrum [14].

The standardization process on IAB started in 2017 by means of a study item for 5G NR within the scope of Release 15. The technical report [15] describes IAB architectures, radio protocols and physical layer aspects considered by that study item. Later, on July 2020, Release 16 was endorsed, in which protocol layers and architecture of IAB were included in the technical specification [16]. Moreover, the minimum IAB radio frequency (RF) characteristics and minimum NR IAB performance requirements were specified in [17].

Different from LTE relaying, NR-IAB provides greater flexibility by enabling multihop architecture, flexible topology, dynamic resource sharing, as well as the possibility of using mmWave bands for both access and backhaul. Specifically, the wider bandwidths on mmWave together with directionality of massive multiple input multiple output (MIMO) make it possible to use aggressive spectrum reuse and reach higher transmit data rates compared to legacy 6 GHz bands. In the following, we provide more details on IAB architecture and features.

A. IAB ARCHITECTURE

The integration of IAB in NR strives to reuse existing functions and interfaces. Figure 2 illustrates the IAB architecture adopted in NR. One important aspect is the support of

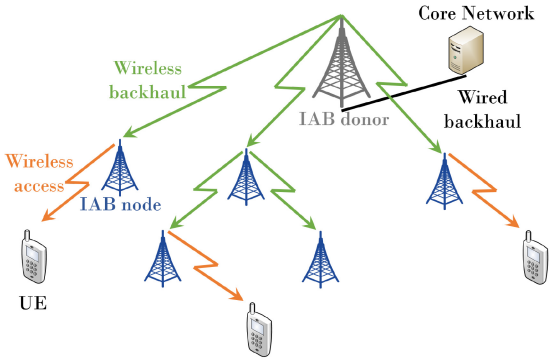

(a) Multiple backhaul hops illustration.

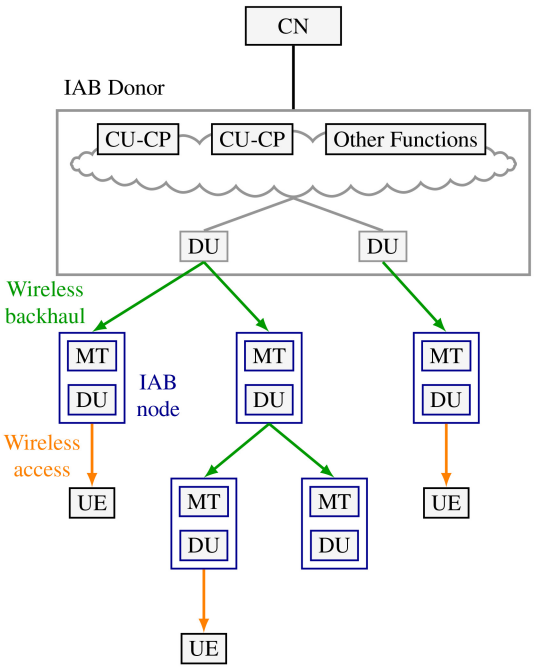

(b) IAB donor and nodes main components.

FIGURE 2. IAB NR architecture.

multiple wireless backhaul hops. This is illustrated in Fig. 2a by the blue BSs, called IAB nodes, which can be wireless connected one to another. In contrast, the terminating gNodeB (gNB), i.e., the gray BS with a wired backhaul and which provides a wireless backhaul to other BSs, is called IAB donor. The IAB NR support of multiple hops helps to overcome two challenges of signal propagation in mmWaves: its limited coverage range and its low capacity to contour obstacles. However, the main challenges to support multiple hops are related to scalability issues, e.g., increased signaling load and uplink (UL) scheduling latency.

Regarding the IAB nodes, they support gNB distributed unit (DU) and mobile termination (MT) functionalities [16], as illustrated in Fig. 2b. On the one hand, the MT part of an IAB node manages the radio interface layers of its backhaul towards an upstream IAB donor or another IAB node. On the other hand, the DU part provides the NR interface to UEs and to MT parts of downstream IAB nodes.

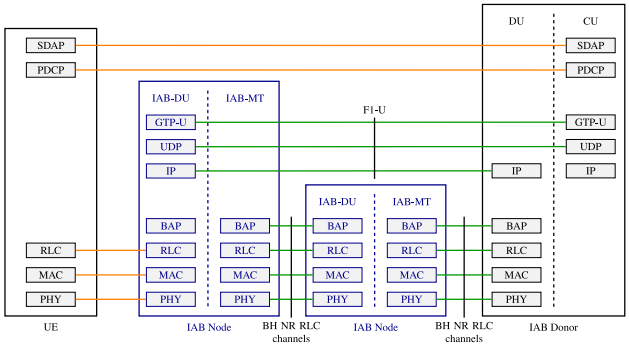

(a) User plane.

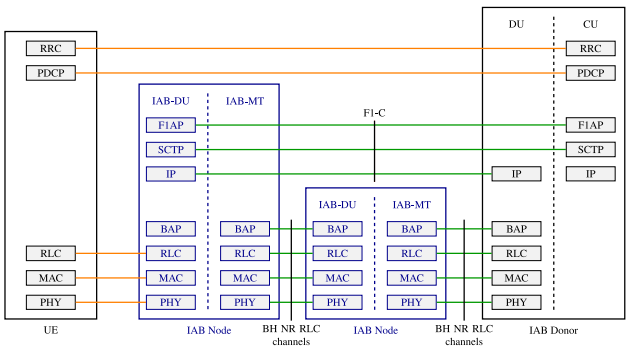

(b) Control plane.

FIGURE 3. Protocol stack.

For compatibility purposes with legacy networks, the MT part of an IAB node acts as a regular UE from the point-of-view of its serving BS (either an IAB donor or another IAB node). From a UE point of view, the DU part of an IAB node looks like as the DU of a regular gNB.

Concerning the IAB donor, it is split in centralized units (CUs) and DUs [16]. This split is transparent to the served nodes and these units can be either collocated or non-collocated. As illustrated in Fig. 3, the DUs are responsible for lower protocol layers, e.g., physical (PHY), medium access control (MAC), and radio link control (RLC), while the CUs provide upper protocol layers, e.g., packet data convergence protocol (PDCP) and service data adaptation protocol (SDAP) / radio resource control (RRC). The main objective of this split is to allow time-critical functionalities, e.g., scheduling and retransmission, to be performed in DUs closer to the served nodes, while other functionalities can be performed in CUs with better processing capacity [18].

B. PROTOCOL LAYERS

As it can be seen in Figure 3, CU and DUs are connected via the F1 interface. The open and point-to-point F1 interface supports both the exchange of signaling information by means of F1-C (control plane), and data transmission between end points through F1-U (user plane) [19]. The main capabilities of F1 interface are the management of radio bearers and backhaul RLC channels as well as the transfer of RRC messages between UE and gNB-CU.

According to [15], IAB backhaul can operate in both in-band and out-of-band scenarios with respect to access links. In in-band mode, there is at least a partial overlap between the used frequency resources by backhaul and access links. However, in this case, IAB nodes cannot transmit and receive at the same time in order to avoid self-interference, i.e., they operate in half duplex (HD). So, the DU part of an IAB node cannot transmit while its MT part is receiving and vice versa. In case of in-band scenario, time division multiplexing (TDM) or space-division multiplexing (SDM) should be employed in order to avoid undesirable interferences. In out-of-band mode, the backhaul and access links use different frequency resources so as to avoid cross-tier interference. time division duplex (TDD) should be employed as NR operators will typically have access to wide bandwidth at mmWave. Thus, the time domain should be properly configured to coordinate transmissions in downlink/uplink for access and backhaul links. The time share for uplink/downlink transmissions in access and backhaul to optimize system performance can be based on the system load, for example.

Backhaul RLC or BH NR RLC channels are responsible for transporting traffic between IAB nodes or between IAB donor and IAB nodes. As the functional CU/DU split occurs at RLC layer, IAB nodes are interconnected at this level. Hop-by-hop automatic repeat request (ARQ) is considered for the RLC layer instead of an end-to-end ARQ. The main disadvantages of hop-by-hop ARQ are the higher packet forward latency (due to the RLC-state machine on each hop) and the lack of guarantee for lossless uplink packet delivery in certain scenarios, e.g., topology adaptation due to link failure. However, end-to-end ARQ at RLC layer leads to latency due to retransmissions that increases with the number of hops. Another drawback of end-to-end ARQ is that a packet loss requires retransmission in multiple links including the ones whose transmission was successful [15]. Multiple backhaul RLC channels can be setup on each backhaul link to assure quality of service (QoS) guarantees. More specifically, there are two types of mapping between UE data radio bearers and backhaul RLC channels: one-to-one and multiple-to-one mappings. In the first case, each UE radio bearer is mapped to a separate backhaul RLC channel, whereas in the second case several UE radio bearers are multiplexed onto a single backhaul RLC channel. On the one hand one-to-one mapping can ensure strict QoS guarantees, but on the other hand multiple-to-one mapping decreases the signaling load and required number of RLC channels that should be established.

One of the premises of IAB standardization is to decrease as much as possible its impact on NR Release 15 specifications. However, in order to support routing across IAB nodes, i.e., control how packets are forwarded among IAB nodes, IAB donor, and UEs, a new protocol sublayer was proposed: the backhaul adaptation protocol (BAP) [20]. In this sense, the BAP sublayer is responsible for efficient forwarding of Internet protocol (IP) packets between IAB nodes on the top

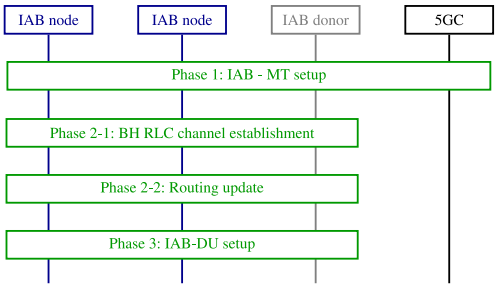

FIGURE 4. IAB node integration procedure [21].

of RLC backhaul channels. In downlink, the BAP sublayer of the IAB donor DU encapsulates PDCP packets that, in their turn, are transmitted through RLC backhaul channels and, finally, de-encapsulated at the DU side of the target IAB node. In uplink, the PDCP packets are encapsulated at the IAB node in the origin and de-encapsulated at the DU part of the IAB donor. Each IAB node owns a BAP address that uniquely identifies it in an IAB network. The header of a BAP packet carries a BAP routing identification (ID) that is setup by the CU part of the donor IAB. The routing ID is composed of a BAP address and a BAP path ID. While the former identifies the destination node where the packet should be delivered, the latter defines the routing path that the packet should follow, if more than one, until reaching the destination node. Therefore, at each node, the BAP header should be inspected in order to determine if the packet has reached its destination or to determine the next hop that the packet should be forwarded to. In downlink, the DU part of the IAB donor is responsible for inserting the header of BAP packets, while in uplink this task is performed by the first IAB node in the route. The routing table used for uplink and downlink can be different from each other.

C. NETWORK PROCEDURES

Regarding integration of new IAB nodes to the system, topology adaptation and IAB resource configuration, 3GPP tried to be as much as possible compatible with legacy procedures and adapted the equivalent procedures of a regular gNB for the case of an IAB node. In the following, we briefly present how these procedures work in the context of IAB.

1) IAB NODE INTEGRATION PROCEDURE

3GPP specified in [21] how a new IAB node is integrated to the system. This procedure is illustrated in Fig. 4 and is split into three phases.

In the first phase, the IAB-MT of the new IAB node connects to the network in the same way as a regular UE with two differences [16]: 1) the IAB-MT ignores cell-barring or cell-reservation indications contained in cell system information broadcast; 2) the IAB-MT only considers a cell as a candidate for cell selection if the cell system information broadcast indicates IAB support. Except for the mentioned differences, the IAB-MT, as a regular UE, searches the frequency band for synchronization signal

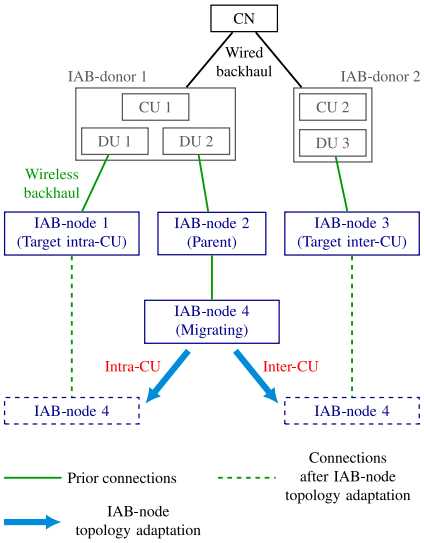

FIGURE 5. Topology adaptation illustration.

blocks (SSBs) in order to identify the most suitable cell. After a successful random access, the IAB-MT performs a RRC connection setup procedure with the IAB donor-CU, authentication with the CN, and context management and radio bearer configuration with intermediary IAB nodes, if any.

The second phase is split into two main parts. The first part concerns the establishment of new BH RLC channel or modification of an existing one between the intermediary IAB node and the IAB-donor-DU. This part also includes configuring the BAP Address of intermediary IAB nodes and default BAP Routing ID for the upstream direction. In the second part, the BAP sublayer is updated to support routing between the new IAB node and the IAB-donor-DU.

Finally, the third phase concerns the configuration of the DU part of the new IAB node. The F1 link between the IAB donor CU and the DU part of the new IAB node is setup with the allocated IP address. After that, the new IAB node is ready to start serving UEs.

2) TOPOLOGY ADAPTATION

After being integrated to the system and connected to a parent node, an IAB node may need to migrate to a different parent node, e.g., when the link towards its current parent becomes weak due to mobility or obstacles between transmitter and receiver. For this, topology adaptation is performed.

Figure 5 illustrates an example where IAB node 4 needs to migrate to another parent. Its serving IAB parent (IAB node 2) and the target one (IAB nodes 1 or 3) may be served either by the same IAB donor-CU (intra-CU) or by a different IAB donor-CU (inter-CU). 3GPP defined in [21] different procedures for each case.

In both intra-CU and inter-CU topology adaptation procedures, first the migrating node (IAB node 4) sends a measurement report to its parent node (IAB node 2). This

measurement report is forwarded from IAB node 2 towards its IAB-donor CU (CU 1) via an UL RRC transfer. The IAB-donor CU is responsible for evaluating if a topology adaptation is required. If so, it chooses a target node to be the new parent of the migrating node.

If the target node (e.g., IAB-node 1) is served by this IAB-donor CU, i.e., CU 1, (intra-CU topology adaptation), this CU directly sends a message to the target node with a `CONTEXT_SETUP_REQUEST`. If CU 1 receives a positive response, it sends a RRC reconfiguration message to IAB node 2 (the current parent), which forwards this message to IAB node 4. IAB node 4 will then perform a random access procedure towards the target parent, i.e., IAB node 1. If everything goes well, the new connection is established, and the migrating IAB node sends a `RRC_RECONFIGURATION_COMPLETE` message to its new parent (IAB node 1), which forwards this message to the IAB donor CU. Finally, the BH RLC channels are configured and the BAP route and mapping rules are updated.

Otherwise, if the target node (e.g., IAB-node 3) is served by another IAB-donor CU (e.g., CU 2 in an inter-CU topology adaptation), then CU 1 sends a HO request via X_n interface to CU 2. Similar to the previous case, CU 2 will send a `CONTEXT_SETUP_REQUEST` to the target IAB node 3 and wait for a response and, if it is positive, CU 2 will send a HO ACK to CU 1. Also similar to the previous case, CU 1 then sends a RRC reconfiguration message to IAB node 2 (the current parent), which forwards this message to IAB node 4. IAB node 4 will then perform a random access procedure towards the target parent, i.e., IAB node 3. If everything goes well, the new connection is established, and the migrating IAB node sends a `RRC_RECONFIGURATION_COMPLETE` message to its new parent (IAB node 1), which forwards this message to its IAB donor CU (CU 2). Finally, a new F1 is established between IAB node 4 and CU 2, the BH RLC channels are configured, and the BAP route and mapping rules are updated.

It is worth noting that, for both cases, the parent IAB-node never directly communicates with the target parent IAB-node. The communication between them is performed through the IAB donor CU. Also, according to [21], in upstream direction of intra-CU topology adaptation, in-flight packets between the source parent IAB node and the IAB donor CU can be delivered even after the target path is established, while, in-flight downlink data in the source path may be discarded, since the IAB donor CU can determine unsuccessfully transmitted downlink data over the backhaul.

3) IAB RESOURCE CONFIGURATION

The deployment of wireless backhaul is a potential source of interference in the system. In order to avoid self-interference and sometimes due to hardware limitations, in general, IAB-DU and IAB-MT operate in HD, i.e., IAB-DU does not transmit at the same time as IAB-MT receives and vice-versa. However, some special cases of IAB-full duplex (FD) are envisioned, e.g., when the antennas of IAB-DU and IAB-MT point towards different directions or the IAB-MT is outside and the IAB-DU is inside [22].

Regarding the direction (transmission or reception) in which the frequency resources are used in the time domain by an IAB-MT, they can be configured via RRC signaling by the IAB node parent as downlink, uplink or flexible. When configured as downlink, it is only used by the parent in the downlink direction (MT reception only). When configured as uplink, it is only used by the parent in the uplink direction (MT transmission only). When configured as flexible, it can be used in either direction (but not simultaneously). Its instantaneous direction is determined by the parent node scheduler.

Similar to the MT frequency resources, the IAB-DU resources can also be configured as downlink (DU transmission only), uplink (DU reception only), and flexible. However, another configuration is also allowed for the DU resources: not available. In this case, the DU is not allowed to use that resource at all.

To coordinate the use of resources by IAB-DU and IAB-MT parts, an IAB-DU resource can be configured by the parent node as hard, unavailable or soft [16]. If configured as hard, the IAB-DU can use it no matter if it is used by the IAB-MT. In this case, the parent node should avoid transmitting/receiving to/from the IAB-MT in this resource. If configured as unavailable, it cannot be used by the IAB-DU, except for some special cases. Finally, if configured as soft, the IAB-DU can use it conditionally either on an explicit indication of availability by the parent node or on an implicit determination of availability by the IAB-DU based on whether or not the use of that resource impacts the IAB-MT. It is the CU‘s responsibility to configure both the parent IAB node and the IAB node such that their respective availability configuration are compatible.

With respect to IAB-MT UL scheduling, increased latency due to multiple hops can adversely impact the system performance. The reason for this is that usually an equipment only requests UL data transmission after it actually receives the data to be transmitted, informed via a buffer status report (BSR). In other words, in a multihop system, the delay is cumulative since an intermediary equipment must first receive the data, before requesting UL resources and finally forwarding the data in UL. To overcome this issue, it was standardized in [16] that an IAB-node can send a pre-emptive BSR to request UL resources, i.e., request UL resources based on expected data rather than on data already buffered. In this case, when data is received by an intermediary IAB node, UL resources are already reserved to be used for forwarding the data to the IAB parent.

D. IAB IN RELEASE 17

The Release 17 Stage 3 functional freeze occurred on March, 2022. A new work item entitled Enhancements to Integrated Access and Backhaul for NR was studied for Release 17 [23]. Its main objectives were [24]:

- Topology adaptation enhancements and routing: Among the main studies in this topic we can mention the specification of inter-donor IAB migration and reduction of the associated signaling load. The main objectives of this topic are the increase of system robustness and load balancing. Moreover, support for CP/UP separation and reduction of service interruption time, e.g., during IAB-node migration, are also envisioned to increase reliability. Remaining studies are focused on multihop latency and congestion mitigation.
- Duplexing enhancements: HD constraint imposes limitations on IAB operation. In this topic, the focus is to improve spectral efficiency and latency by supporting simultaneous operation of IAB node's child and parent. In this case, it is possible that the MT part of an IAB node could transmit while the DU part of the same node could be receiving, i.e., FD mode. Another possibility is the simultaneous transmission or reception of MT and DU parts by leveraging spatial multiplexing techniques. Furthermore, dual connectivity scenarios should be considered so as to improve robustness and perform load balancing.

III. OVERVIEW ON FIXED IAB

A. TAXONOMY ON FIXED IAB

Thanks to the great flexibility of IAB networks, the existing literature on fixed IAB can be categorized under many different criteria. In this section, we provide a taxonomy of the works on IAB according to the following criteria:

1) Studied dimensions and article profile: the system performance on IAB networks can be improved by optimizing different aspects. In this criterion, the works can be characterized according to the functionalities that are studied. The considered categories are surveys, overview, testbeds, IAB versus fiber-based network performance, network deployment, routing and topology adaptation, resource allocation for access and/or backhaul, power allocation, UE association and MIMO beamforming;
2) System modeling assumptions and constraints: depending on the dimensions that are being optimized in each article, the authors can make some assumptions about the system model that can boost performance but, at the same time, can turn the problems harder to solve. In this criterion, we consider the following categories: FD, intelligent reflecting surface (IRS), multihop, multiple antennas, UE-centric approach, modeling of both uplink and downlink, modeling of access and backhaul links, mesh topology and non-orthogonal multiple access (NOMA);
3) Problem objectives and KPIs: the performance of IAB networks can be measured under different points of view, therefore, different objectives and metrics are optimized in the reviewed articles. In this criterion, we assume the following categories: fairness, latency, spectral efficiency, energy efficiency, data rate guarantees for UEs, coverage probability, weighted sum rate, and symbol error rate;
4) Solution approaches and mathematical tools: in this criterion, the works can be classified according to the employed tool in order to solve the studied problem(s). Among the common tools we can mention: convex optimization, linear (continuous) optimization, integer linear optimization, heuristics, dynamic programming, machine learning and metaheuristics, stochastic optimization, game theory, stochastic geometry, and statistical analysis.

Note that, depending on the assumed criteria, the same work can be classified in more than one category. In the following section, we describe some important works on fixed IAB clearly identifying the classification according to the established criteria.

B. LITERATURE REVIEW ON FIXED IAB

In Figure 6, we present the taxonomy for the reviewed articles in fixed IAB assuming the four abovementioned criteria. For the sake of organization, the works are presented in the following according to the first criterion.

1) SURVEYS, OVERVIEW PAPERS, TESTBEDS, AND IAB VERSUS FIBER-BASED NETWORK PERFORMANCE

The works [10], [14], [18], [25], [26], [27], [28], [29], [30], [31] provided an overview of IAB technology by describing several aspects regarding architecture, protocol aspects and/or physical layer. More specifically, [10] provides a survey on fixed IAB. Its authors classified IAB works in the following groups: stochastic geometry-based works, resource allocation, scheduling, cache-enabled IAB networks, optical IAB networks and non-terrestrial IAB networks. The works [27], [31] presented a proof of concept of a two-hop IAB network using two-sectors IAB nodes operating at mmWave. In [26], a testbed was presented composed of a donor BS, an IAB node and a UE.

The works [14], [18] as well as [29], [32], [33], [34] presented simulation results of IAB networks versus fiber-based networks. Some of the conclusions that can be gathered from those works is that IAB performance is close to the one of all-wired networks for low and moderate traffic, and that the performance of fully-fiber connected networks can be achieved with a small increase in the number of IAB nodes in IAB networks. Moreover, they showed that IAB is a relevant technology for 5G since it allows to incrementally improve the fiber density in the network.

2) NETWORK DEPLOYMENT, ROUTING AND TOPOLOGY ADAPTATION

Network deployment, routing and topology adaptation were studied in [14], [28], [32], [35], [36], [37], [38], [39], [40], [41], [42], [43], [44], [45], [46], [47], [48]. In general, for a broad range of coverage constraints/blockage

Criteria for taxonomy	Categories	Works
Studied dimensions and article profile	IAB overview	[10], [14], [18], [25]–[31]
	IAB performance versus fiber	[14], [18], [29], [32]–[34]
	Survey	[10]
	Testbeds	[26], [27], [31]
	Network deployment, routing and topology adaptation	[14], [28], [32], [35]–[50]
	Resource allocation for access and/or backhaul	[18], [34], [39], [42], [46], [48], [49], [51]–[59]
	Power allocation	[41], [42], [45], [46], [54], [55], [57], [60]
	MIMO beamforming	[30], [54], [61]–[64]
	UE association	[34], [46], [54], [61]
System modeling assumptions and constraints	Full duplex nodes	[30], [41], [42], [45], [56], [57], [61], [64]
	IRS	[47]
	Multihop	[14], [27], [29], [32], [35]–[38], [40]–[49], [53], [58], [59]
	Muliple antennas at IAB nodes	[14], [18], [26]–[30], [32], [35]–[39], [41], [42], [46], [48], [54], [58], [61]–[64]
	User-centric approach	[32], [40], [41], [54], [61]
	Uplink and downlink modeling	[26], [29], [32], [37], [42], [44], [58], [63]
	Access and backhaul links modeling	[14], [18], [26], [27], [29], [30], [32]–[36], [41], [42], [44], [46]–[48], [51]–[59], [61], [63], [64]
	Mesh topology	[32], [37], [38], [43], [44], [47], [53]
	NOMA	[45], [55]
Problem objectives and KPIs	Fairness	[32], [37], [38], [41], [48], [53], [54], [56], [57]
	Latency	[14], [33], [35]–[37], [39], [41]–[44], [58]
	Spectral efficiency	[27], [30], [33], [35], [36], [40], [42]–[44], [49], [62], [64]
	Energy efficiency	[45], [55]
	Data rate guarantees or UEs	[14], [29], [55], [58], [59]
	Coverage probability	[18], [26], [28], [34], [47], [50]–[52], [60], [63]
	Weighted sum rate	[46], [54], [61]
	Symbol error rate	[47], [64]
Solution approaches and mathematical tools	Convex optimization	[32], [41], [43], [46], [53]–[55], [57], [61], [62]
	Linear (continuous) optimization	[37]–[39], [48], [49]
	Integer linear optimization	[37], [39]
	Heuristics	[14], [26], [27], [29], [30], [33], [35], [36], [40], [42], [44]–[46], [48], [54], [58], [61], [63], [64]
	Dynamic programming	[40], [43], [59]
	Machine learning and metaheuristics	[28], [41], [56], [60]
	Stochastic optimization	[41], [61]
	Game theory	[53]
	Stochastic geometry	[18], [28], [34], [51], [52]
	Statistical analysis	[47]

FIGURE 6. Taxonomy for fixed IAB: studied dimensions and article profile, system modeling assumptions and constraints, problem objectives and KPIs, and solution approaches and mathematical tools.

densities, the impact of meshed communication to increase redundancy may be negligible if the network is well planned.

In [32] the authors studied a convex optimization problem with the objective of maximizing the product of UEs' downlink and uplink data rates (geometric mean) subject

to capacity and resource allocation constraints. Two IAB topologies were considered: mesh and spanning tree based on highest channel quality among IAB nodes. Simulation results showed that the presented mesh topology improved data rate fairness slightly.

Mesh topology was also studied in [44] for IAB networks. The authors proposed a mesh topology for IAB networks where the split DU/MT in IAB nodes is replaced by a peer unit. Each peer unit of an IAB node can be dynamically configured as master or slave. An IAB node configured as master can control their links to other IAB nodes configured as slaves as well as its own access links. Simulation results showed that the proposed mesh topology provides lower packet delays and significant total throughput gains. Mesh networks for IAB were also studied in [43] where the authors studied the problem of maximizing the number of delivered broadcast packets. Optimal and suboptimal solutions were proposed. Mesh IAB with IRSs was studied in [47]. The authors reported that the use of IRSs is capable of improving signal to noise ratio (SNR) and symbol error rate (SER), which allows for the use of higher modulation orders, and that outage probability for multiple hops can be reduced if the number of elements in IRS is increased. However, it is important to highlight that none of the works presented in this section about mesh topology included in their analysis the increased complexity of enabling a mesh architecture in IAB networks in terms of signaling overhead, for example.

The authors in [45] considered a heterogeneous network and studied the problems of power allocation and routing. In this work, they assumed cooperation between BSs that can employ orthogonal multiple access (OMA) and NOMA multiple access schemes. The main outcome of this work was the proposal of a joint and adaptive greedy routing solution that switches between cooperative OMA and NOMA in order to maximize energy efficiency subject to data rate and power constraints.

In [36], the authors studied distributed routing strategies (path selection) for IAB networks. Four routing solutions were presented: highest-quality-first, wired-first, position-aware and maximum-local-rate policies. In the highest-quality-first solution, the next hop is the one that presents the highest signal to interference-plus-noise ratio (SINR) whereas in the wired-first one, the chosen hop is the one that provides the shortest path to the IAB donor. The main idea in the position-aware policy is to achieve a balance between highest-quality-first and wired-first solutions. Finally, the maximum-local-rate solution chooses the next hop with highest data rate that, in its turn, takes into account the number of connected UEs in the parent IAB node, i.e., IAB load. Performance results showed that the wired-first policy provided a reduced number of hops at the cost of lower worst-SINR. Similar routing solutions and some new variants were evaluated in [14], [35]. In [14], the authors showed that choosing wired-first routing instead of highest-quality-first routing provides higher throughput and lower latency. In [35], the reported results showed that although the highest-quality-first routing improved the link quality at backhaul and access links, the number of hops to the core network has increased. Strategies based on path data rate, i.e., end-to-end data rate, were able to reduce the number of hops to the core network.

Topology formation and adaptation for IAB networks were evaluated in [40]. Optimal and suboptimal solutions were proposed for a topology formation problem that maximizes the minimum capacity across the system. As conclusion, this work showed that for few IAB nodes, all algorithms achieved a similar performance since the number of options for topology formation is not high.

3) RESOURCE ALLOCATION FOR ACCESS AND/OR BACKHAUL

As opposed to out-of-band operation where the access and backhaul operate in different frequencies, in-band backhauling refers to the cases with the access and backhauling sharing the same resources. Compared to out-of-band backhauling, in-band operation leads to higher flexibility at the cost of complexity. The state-of-the-art works concentrate mainly on in-band backhauling [18], [34], [39], [42], [46], [48], [51], [52], [53], [54], [55], [56], [57].

The work [34] is an extension of [51]. The bandwidth split between access and backhaul based on a fixed factor proposed in [51] is called orthogonal resource allocation (ORA) in [34]. In this work, the authors proposed an alternative solution called integrated resource allocation (IRA) where the bandwidth assigned by a donor IAB to the backhaul for a given IAB node depends on the access load of the IAB node. Simulation results showed that the coverage probability in ORA is highly dependent on the bandwidth split factor. As the number of small BSs increases, more bandwidth should be reserved to backhaul in ORA scheme. Coverage probability provided by IRA is better than the one achieved with the static ORA scheme.

Resource allocation for access and backhaul was also studied in [42]. In this work, the resource allocation subproblem took the form of defining the spatial multiplexing for the links, i.e., space-division multiple access (SDMA) groups, and the number of slots from the frame assigned to each group. SDMA groups were chosen by using a greedy algorithm based on graph theory. The definition of the number of slots followed a proportional fair policy. In the simulation results, the authors showed that the proposed scheme is more robust than baseline solutions when the number of UEs is increased thanks to the spatial multiplexing capacity.

In [54], the problems of user association, hybrid beamforming (HBF) design, power allocation and resource allocation were studied. A weighted sum rate maximization problem with limited channel state information (CSI) subject to beamforming, power and backhaul constraints was formulated. Due to the complexity of the formulated problem, the authors followed a two-stage approach. At stage 1, user association and beamforming are designed for access links. After that, in stage 2, the decisions for access links are signaled

to the macro BS that in its turn solves resource allocation and beamforming problems for backhaul links. Simulation results showed that the time fraction assigned to access links increases as a result of higher transmit power at macro BS. On the other hand, the increase of the transmit power of small BSs results in a lower time fraction for access links.

Downlink subchannel allocation for access and backhaul in a two-hop IAB network was studied in [56]. The nodes are assumed to be FD-capable and a single antenna is assumed for DU and MT parts. An optimization problem was formulated with the objective of maximizing a utility function (later set to proportional fairness) subject to data rate guarantees for UEs. A learning-based solution was proposed and, according to simulation results, it outperformed the static full-reuse solution in terms of fairness.

In [46], the authors showed that the performance gains of centralized solutions, where most of the resource allocation decisions are taken on IAB donors based on channel quality information sent from child nodes, is strongly dependent on the effect of channel aging. Channel aging is caused by the fact that the channel quality considered by donor IAB may considerably change when resource allocation decisions are actually employed by child nodes. Other works, e.g., [39], [42], [46], [48], also considered centralized solutions.

Although fully centralized scheduling is not 3GPP compliant for IAB, nodes can exchange information and, eventually, it can be assembled in a central node that reports general recommendations for resource allocation and scheduling to the other network nodes. This is the key idea of [58]. In [58], a central controller receives general information about network nodes, e.g., CSI and buffer status, and provides centralized recommendations for resource partitioning to the distributed schedulers. However, the local DUs are free to follow or not the indications of the central controller depending on local conditions. One important conclusion of this work is that this semi-centralized framework provides performance gains, however, it strongly depends on the capacity of the system in exchanging information in a timely manner.

The works [18], [34], [51], [52], [54] present resource allocation and scheduling solutions that can be classified as a semi-centralized operation where partitioning of bandwidth between access and backhaul is taken in a central node based on the available system information, but the proper association among system resources and links is decided locally.

In [49], the authors proposed a distributed/decentralized solution to scheduling/resource allocation problem. The proposed solution takes advantage of the information spread by network nodes about the bandwidth allocated to their children as well as the local perspective obtained about network topology. Based on this information, local optimization problems are solved at each node for resource allocation.

Finally, in [59] the authors proposed distributed schedulers for multihop IAB assuming a limited number of RF chains. An optimal back-pressure scheduling solution as well as a distributed message passing scheme were proposed in order to achieve queue stability. Furthermore, another contribution of [59] was the proposal of local schedulers with a simplified exchanging of messages among nodes.

4) POWER ALLOCATION

Power allocation may be useful for the cases with simultaneous operation at the IAB node, especially if the network deployment is not well planned. For this reason, power allocation has been discussed in 3GPP Release 17 work-item on IAB enhancements. Power allocation was also studied in [41], [42], [45], [46], [54], [55], [57], [60]. With exception of [60], it is important to note that power allocation was not studied alone in those works; in fact, power allocation was jointly studied with resource allocation for access and/or backhaul, routing/topology adaptation or UE association. Routing and power allocation was studied in [41]. The main outcome of this work was that power allocation leads to only marginal improvements in the delay performance when intelligent routing is already considered. Power allocation for SDMA groups and assuming fixed routing was also studied in [42] with the objective of maximizing spectral efficiency.

In [57], the authors decoupled the original optimization problem in bandwidth and power allocation for maximizing the proportional fairness in the system. After solving bandwidth allocation, the transmit power allocation for downlink was solved for access and backhaul independently since there are no coupled constraints. From the simulation results, the authors showed that throughput can be increased until a certain level as the downlink access transmission power is augmented. For higher access transmission power, the backhaul capacity starts to limit the UEs' data rates.

Besides bandwidth allocation, power allocation was studied in [55] with the objective of maximizing energy efficiency. The bandwidth and power allocation original problem for downlink was solved by leveraging fractional programming properties and sequential convex approximation. The authors showed in the simulation results that energy efficiency increases with the macro BS's transmit power, however, the high transmit power at small BSs leads to a higher power consumption per data rate which results in poor energy efficiency.

Simulation results showed that, as the number of relaying small BSs is gradually increased, the performance of cooperative OMA and NOMA in terms of energy efficiency and power consumption is improved until a certain point. Moreover, results showed that joint cooperative OMA and NOMA enjoys the benefits of both cooperative OMA and NOMA and presents better performance in different conditions.

Joint power allocation and subcarrier assignment for downlink were considered in [46] for a multihop IAB network. As different subbands were assigned to each backhaul link and access, power allocation was optimally derived for subcarriers within each subband. Suboptimal power allocation solutions were also provided, which showed negligible

performance loss to the optimal solutions according to simulation results.

In [60], uplink power control for dual-hop IAB networks was studied. The main objective of the power control solution was to maximize the coverage probability by employing genetic algorithm (GA). Simulation results showed that power control is able to substantially improve the coverage probability especially when out-of-band IAB is used. Also, the authors showed that inter-cell interference does not play an important role since mmWave band was assumed and, thus, signal strength quickly decreases with distance.

5) MIMO, BEAMFORMING AND UE ASSOCIATION

The impact of UE association is considerably different in IAB networks when compared to conventional fiber-based networks. The main reason is that the load of UEs transferred from donor IAB to IAB nodes comes back to IAB donors through the backhaul. Thus, UE association and load balancing should be re-thought for IAB networks. Moreover, multiple antennas technology, that is a key aspect for 5G, assumes a relevant role in IAB networks since backhaul data rates should be in the order of the total access data rate of IAB nodes. Spatial multiplexing between access and backhaul links is also another aspect that has the potential to increase IAB efficiency. In the following, we present some important works related to this topic.

The proper connection between UEs and BSs, i.e., UE association, was investigated in [34], [46], [54], [61]. In [34], the criterion to define which BS a UE should connect to is based on the highest product between the received power and a constant bias. In the simulation results, the authors showed that, as the bias factor of IAB nodes increases relative to the one of IAB donors, more UEs are offloaded to the IAB nodes, thus increasing the load in backhaul links.

In [62], the authors focused on MIMO for backhaul links. The expected spectral efficiency for wireless MIMO backhaul links is much higher than in MIMO access links. Therefore, physical impairments such as time offset, which can lead to inter symbol interference (ISI), and phase noise that increases the multi-access interference due to outdated precoder and decorrelator should be carefully mitigated for backhaul links. The main contributions of the article were the proposal of a time offset compensation, phase noise estimation and design of a precoder/decorrelator.

In [63], the authors investigated the impact of the arrangement of antennas in tri-sectorized IAB nodes. In order to decrease inter-sector interference and allow the reuse of frequency resources in different sectors of the same IAB node, two strategies are employed: spatial and angular diversities. In the first one, the arrays of antennas of each sector are disposed in the vertices of an equilateral triangle whereas the IAB node equipment are located in the center of mass of the triangle. In the second strategy, a minimum angular separation should be kept between UEs associated to adjacent sectors of the same IAB node.

FD-IAB nodes with subarray-based HBF scheme were considered in [30]. By assuming that antenna isolation and RF cancellation are perfect, the authors designed digital filters to mitigate residual self-interference (with minimum mean square error (MMSE) combiner) at the IAB receiver and multi-user interference at transmitter (with zero-forcing (ZF) precoder). The proposed scheme is evaluated through simulations by varying channel estimation errors and RF insertion losses, i.e., losses in phase shifters, power dividers and power combiners in mmWave. Simulation results showed the spectral efficiency gains of FD versus HD IAB transceivers as well as showed that the proposed scheme experiences less RF insertion loss than the fully-connected HBF. However, it is important to highlight that the actual implementation of FD technology in IAB nodes is still very challenging especially due to self-interference issues.

In [64], a further study of the same authors from [30], the authors assumed a fiber Bragg grating-based analog canceler that is placed before RF precoding and after RF combiner. Reduced bit error rate (BER) was observed in the simulation results when compared to baseline schemes.

IV. MOBILE IAB

Wireless backhaul may allow the deployment of mobile cells, i.e., mIAB, which can hopefully provide uninterrupted cellular services for moving UEs, e.g., passengers in buses.

The concept of mobile cells is not new. mobile relay nodes (MRNs) were already studied in the past with a similar purpose. It has even been addressed by 3GPP Release 12 in [65]. The focus of [65] was on high speed trains with known trajectory. In the considered topology, outer antennas of access devices, e.g., installed on the top of the train, provide wireless backhaul connection via the evolved node Bs (eNBs) mounted along the railway, while inner antennas installed inside are responsible for providing wireless connectivity to the passengers. Important to highlight that these devices support multi-radio access technology (RAT) functionalities. It means that, while the backhaul link works over LTE, the access link can be deployed over other technologies, e.g., wireless fidelity (Wi-Fi).

A recent technical report from 3GPP [66] presents a study on several use cases and requirements for 5G networks for mobile BS relays mounted on vehicles, i.e., vehicle-mounted relays (VMRs). The study item is part of initial studies for Release 18. The use cases cover many aspects including service provision for both onboard UEs and UEs in the vicinity of the vehicle as well as seamless connectivity in different scenarios involving mobility of UEs and relays.

Works related to mIAB, moving relays and moving cells can be classified according to different criteria. Fig. 7 presents the classification adopted in the present survey. The works are first grouped based on the existence or not of non-terrestrial links. Works of both groups, i.e., terrestrial and non-terrestrial, are classified according to the type of considered network nodes, e.g., train, bus, UAV, etc. This is due to fact that works considering similar network nodes

		Main Topic	Out-of-Band (or not mentioned)	In-Band
Terrestrial	General	Overall system	[11], [65]	
		Channel estimation	[67]–[70]	
		Probability of outage		[71], [72]
		Energy efficiency	[73]	[74]
		Resource allocation		[75]
		Interference management		[76]
		Resource allocation		[77], [78]
	Train	Overall system	[79]–[81]	[82]
		Field trial	[83]	[84]
		Power allocation	[85]	
		Power allocation	[86]	
		Beamforming design	[87]	
	Bus	Interference management Resource allocation	[88]–[92]	[93]
		Interference management Resource allocation Power allocation		[94]
		Handover	[95]	[96]
		Handover Bandwidth allocation	[97]	
Non-Terrestrial	UAV	General	[98]	[99]
		Caching content	[100]	
		Optimal position	[101]	[102]
		Optimal position UE association	[103]	
		Optimal position UE association UE power allocation		[104], [105]
		Optimal position UE association Bandwidth allocation		[106], [107]
		Optimal position UE association UE power allocation Bandwidth allocation		[108]–[110]
	Satellite	Overview	[111], [112]	[113]
		Resource allocation		[114], [115]
		UE offloading	[116]	
		Adaptive RF	[117]	
		Physical layer security	[118]	
		Integration with vehicular networks	[119]	
		Architecture for AI integration	[120]	

FIGURE 7. Taxonomy for mobile IAB: types of mobility and studied topics.

usually consider similar problems, e.g., UAV positioning, and take advantage of specific characteristics of each type of node, e.g., previously known mobile trajectory of buses. Furthermore, works considering different types of nodes usually consider different environments, e.g., while bus related works try to improve in-vehicle UEs QoS taking into account

the presence of out-of-vehicle UEs, train related works only consider the presence of in-vehicle UEs. For each type of network node, we present the most recurrent topics and solutions present in the literature.

Fig. 7 also classifies the works based on whether access and backhaul are in-band or out-of-band (or if this aspect is not mentioned). On the one hand, considering access and backhaul links operating either in different frequency spectrum or technologies simplifies two of the main challenges related to wireless backhaul and moving cells: managing the resources between access and backhaul links and dealing with the dynamic interference between moving cells and crossed fixed cells. On the other hand, using the same technology and frequency spectrum for both access and backhaul links may result in efficient system operation and optimized use of the scarce and expensive frequency spectrum, respectively.

In the following, a literature review of the main topics related to mIAB is presented considering the taxonomy presented in Fig. 7.

A. TERRESTRIAL

1) GENERAL

Regarding terrestrial mIAB, before presenting works that take into account characteristics specifics of a given mIAB node, e.g., a bus or a train, we present works that consider vehicles in general without assuming any characteristic of a particular vehicle.

The work [67] is a fundamental article that proposed a way to deploy a set of antennas in a vehicle to allow transmissions with good signal quality to and from mobile nodes. The authors of [67] proposed an MRN setup configured with two groups of antennas on the roof of a vehicle: 1) the front predictor antennas; and 2) the back receive antennas. In this way, the CSI acquired by front predictor antennas is exploited for data transmission to the behind receive antennas when they reach the same position, and the channel aging effect is minimized. If the receive antennas end up in the same position, it will experience the same radio environment, and the CSI will be almost perfect. If the receive antennas do not reach the same point as the predictor ones, due to, e.g., the processing delay is not equal to the time needed until the receive antennas reach the same point as the predictor ones, the receive antennas may receive the data in a place different from the one where the predictor antennas sent the pilots. Such spatial mismatch may lead to CSI inaccuracy, which deteriorates the system performance. Different methods based on transmission delay adaptation or rate adaptation are proposed to reduce the effect of spatial mismatch.

Similar to [67], other works from the literature have also already investigated the topic of predictor antennas from a theoretical perspective, e.g, [68], [69], and as experimental testbeds, e.g., [70].

The authors of [71], [72] analyzed the end-to-end outage probability and capacity at a vehicular UE of single-hop direct transmission (baseline case), and dual-hop transmission via an MRN as well as a fixed relay node. They assumed that the downlink of different cells were synchronized, where the backhaul links were only active in the first time slot and access links were only active in the following slot. Thus, backhaul links and access links did not interfere with each other. By theoretical analyses and computational simulations the authors showed that in the cases of moderate to high vehicle penetration loss, MRNs deployed on top of vehicles enhanced QoS of the vehicular UEs compared to the scenarios with only direct transmission and with fixed relay nodes.

In [74], the authors of [71], [72] extended their study and compared the required average transmit power in similar scenarios under an outage probability constraint. They showed that dual-hop transmission via an MRN can also significantly reduce the power consumption of the network.

As the authors of [74], the authors of [73] also addressed the topic of energy efficiency. They proposed a Q-learning-based scheme to stabilize the energy efficiency of IAB nodes backhaul. For this, each mIAB node, i.e., vehicle-mounted access points (APs), periodically reported its location and velocity to an access controller. The access controller was responsible for predicting the most suitable BS or device-to-device (D2D) node to serve the IAB nodes in the future and for configuring them to be connected to the predicted BS or D2D node. The IAB nodes, in their turn, were responsible for selecting a suitable transmission beamwidth and transmission power that kept the energy efficiency above a given threshold. The selection was performed by using a Q-learning based solution.

The resource allocation for macrocell UEs and the backhaul of the existing and newly arrived moving small cells deployed in vehicles was studied in [75]. The authors formulated the problem of maximizing the downlink data rate of the newly arrived moving small cells in the macrocell such that the data rate of the macrocell UEs and existing moving small cells UEs is protected. They proposed an adjustable-power-based resource allocation to allocate RBs and power in the macrocell.

The problem of resource sharing between moving cells and access links was also studied in [77]. More precisely, they considered a typical mobile cell scenario, where in-vehicle cellular UEs are served by an in-vehicle antenna over the access link. A separate external antenna connects the mobile cells to the nearest eNB over the backhaul link, and to the neighboring mobile cells over the sidehaul link. The authors proposed algorithms to enable resource sharing between a mobile-cell, access link, sidehaul link and conventional cellular users taking into account interference caused by the wireless backhaul of mobile cells. The algorithms' performance was compared with the optimal, yet time-consuming, brute-force method and presented good results based on Monte-Carlo simulations.

The work [77] was extended in [78]. The authors proposed new resource sharing and user scheduling algorithms that

jointly aimed at ensuring that the access link shared the subchannel either with backhaul link or with the out-of-vehicles macrocell UEs. They took into account results from [93] and [94], such as the minimization of interference to backhaul link and provisioning of high QoS for in-vehicle users by considering the use of directional access link antenna even at low transmit power. The authors also exploited the vehicular penetration loss along with self-interference-coordination to further reduce interference between the resource sharing links. They pointed as interesting direction for future research the deployment of the backhaul link for mobile cells through UAVs.

The problem of mutual interference between macro and moving small cell UEs is highlighted in [76]. Its authors studied the impact of deploying moving small cells in a Manhattan grid scenario in the presence of stationary traffic hotspot inside a macro cell. Simulation results showed that deploying moving small cells to offload traffic in the congested macro cell can be beneficial. However, when the small cells were moving far away from the traffic hotspot, the system performance was degraded compared to a network composed of only macro cells due to the high mutual interference between macro and small cell users.

2) TRAIN

Mobile cells deployed at trains is a typical use case of terrestrial mIAB. Due to the high speed and shielding effect of the trains, it is challenging to continuously serve onboard UEs from outside BSs. With the purpose of reducing the penetration losses caused by the Faraday cage characteristics of a high-speed railway (HSR), state-of-the-art works, e.g., [79], [82], [83], [85], [86], usually consider that the MRNs are deployed on top of the carriages and connected to in-cabin wireless APs. The MRNs communicate with BSs, playing the role of forwarding data between the passengers on the train and the broadband wireless networks. Furthermore, since the trains follow a predefined track and pass through uninhabited areas, a common solution is to deploy the external BSs along the railway.

Works [79], [81], [82] provide a review on communication on HSR. The authors of [79], summarized key challenges and provided a review of techniques used to address the listed challenges. They focused on physical layer operations covering modeling and estimation of fast time-varying fading channels, Doppler diversity transmissions and non-coherent detections. However, they also presented discussions on higher layer operations, e.g., HO management, control/user-plane decoupling and network architecture. One of the discussed architectures is the one deploying relays on the roof connected to access points installed inside the train through wired links. The MRNs act as intermediate nodes between inside UEs and external BSs. Since the MRNs are installed outside of the trains, they eliminate the penetration loss. It was highlighted that MRNs can also solve the problem of a high number of simultaneous HO requests, since the HO is performed only between an MRN and an eNB, instead of between multiple UEs and an eNB. That paper did not present either results or more details about the deployment of the MRNs, e.g., central frequency carrier.

In [82], current trends of wireless communications for smart railways were presented. The authors proposed a network slicing architecture for a 5G-based HSR. Similar to [79], in the proposed architecture, APs on the train aggregated the data from different UEs, and relayed them to external BSs through a wireless backhaul. The authors presented simulation results comparing a MIMO-BS-only architecture with the wireless backhaul architecture. However, the simulated scenario was simplified. The train traveled a small distance, less then 10 times its length, and there was only one MIMO-BS positioned in the middle of the path. They highlighted that, for velocities larger than 360 km/h, it is a challeging task to deploy APs on the train or along the track to make a seamlessly connected heterogeneous network and establish a UE association model for service provisioning.

The work [81] describes the main characteristics and requirements for critical and non-critical communications in railways that must be addressed by 5G. The authors highlighted the shielding effect of the train to radio signals, due to its metallic construction. They mentioned that this effect has been quantified in 20-30 dB and therefore, it is necessary to use moving cells for internal network provisioning of reliable communications. They also highlighted the importance of using satellites since high speed lines can travel across large uninhabited areas. Therefore, the trains must be equipped with antennas with mechanical or electrical control.

In [83], [84] results from real measurements are presented. In [84], the authors presented an overview of field trials to assess technical and operating conditions of a 5G mobile communication system capable of supporting high-speed 2 Gbps throughput for HSR. The trials were performed on 2018 in Japan. Two 5G eNBs were deployed operating at 27.875 GHz with bandwidth of 700 MHz and 2 antenna units each with 96 antenna elements in each unit. Concerning the mobile equipment, it was mounted inside the train car, on the front windshield in front of the driver's seat with 64 antenna elements. A maximum throughput of 2.08 Gbps was verified when the train was moving at a speed of 90 km/h.

In [83], the authors deployed an experimental setup for a proof-of-concept. In order to implement a HO-free communication of up to several tens of kilometers, they installed remote antenna units (RAUs) along the railway track and connected them to a central station. The RAUs were responsible for providing a wireless backhaul (75-100 GHz) to a mobile BS installed on a train. UEs on the train communicated with the BS inside the train. They assumed that the train information, e.g., location, velocity, and list of identified BSs, was available at an operation center. This information was utilized to control and switch radio cells instead of using control signals as in cellular networks. They successfully transmitted approximately 20 Gbps and 10 Gbps in downlink (DL) and UL, respectively.

Since the trains' internal network is almost considered as an independent network, state-of-the art works usually focus on the backhaul link between the train antenna and external BSs, as is the case in [85], [86], [87]. More specifically, in [85], the authors investigated the power allocation problem between BSs and MRNs deployed on trains with the objective of maximizing system achievable sum rate. The proposed power allocation algorithm was based on multi-agent deep recurrent deterministic policy gradient, which is capable of learning power decisions from past experience instead from an accurate mathematical model. Simulation results showed that the proposed solution outperformed other state-of-the-art solutions based on machine learning.

Finally, in [87], the authors investigated HBF design for train-to-ground communications. They developed a two-stage algorithm in blockage-free scenarios. In the first stage, the MMSE method was adopted for optimal HBF design with low complexity and fast convergence. In the second stage, the orthogonal matching pursuit method was utilized to approximately recover the analog and digital beamformers. For blocked scenarios, they designed an anti-blockage scheme by adaptively invoking the proposed algorithm. Simulation results showed that the proposed algorithm outperformed state-of-the-art solutions in terms of sum rate for different speed values and blockage probability.

3) BUS

In the context of mIAB considering buses, the majority of the works available in the literature focus on how to allocate resources in order to avoid the interference between access link of inside and outside UEs. A common adopted strategy is to split UEs into inside and outside UEs and allocate them in different parts of the spectrum. Another topic also addressed in the literature is related to HO from two perspectives: how to avoid multiple HOs due to the mobility of the UEs and how to optimize the HO process considering that multiple UEs might change its serving base station (sBS) at the same time since they are moving together. In the following, we briefly discuss some papers.

The authors of [90], [91], [92] considered a macrocell with several public vehicles embedded with mobile femtocell access points (MFAPs). They proposed to deploy mmWave communications at 60 GHz inside vehicles for access links while the backhaul link of MFAPs and the direct link between an external UE and the macro cell use LTE. The authors analyzed three critical cases: a) the bus was near the eNB; b) two buses were close together; and c) an outside UE was close to a bus. They verified that, in case a), the eNB was a big interferer for inside UEs, because its transmission power was higher than that of the MFAPs. UEs served by the MFAPs measured a low SINR, and were forced to disconnect from MFAPs and connect to the eNB. This resulted in a high number of simultaneous HOs. However, as the bus moved, as soon as the signal of the MFAPs was acceptable, UEs had to re-engage to the MFAPs. In the case c), they showed that an outside UE in the proximity of a bus, especially when it was away from the sBS, could connect to the MFAPs, but its connection only lasted for a few minutes, depending on the speed of the bus.

Similar to [90], [91], [92], the authors of [89] considered moving femtocell deployed inside buses. The authors proposed a dynamic frequency allocation scheme that allocates the same frequency band for inside UEs even if they are in different buses, while the outside UEs are allocated in a different frequency band.

In [88], the authors also considered small cells deployed on the buses to serve the passengers. They studied the interference between moving small cells and proposed a probabilistic graph based resource allocation (PGRA) algorithm considering that the path of the moving small cell is fixed but it moves at non-uniform speed.

Different of [88], [89], [90], [91], [92], [93] proposed a model to allow the downlink backhaul sub-channels to be shared by in-vehicle downlink access link. This model is based on vehicular penetration effect and LOS communication. While vehicular penetration depends upon the material and construction properties of the transport vehicle, the LOS communication can be enabled using directional antennas. This paper also advocated that construction parameters and antenna positioning inside vehicles should be considered for future transport vehicles to increase the spectral efficiency for cellular network.

The authors of [93], extended their study in [94]. They presented new results regarding the exploitation of vehicular penetration effect and LOS communication to allow the downlink backhaul sub-channels to be shared by in-vehicle downlink access link transmission. Furthermore, a technique for access link power control was also proposed to reduce the interference to the backhaul link, while maintaining high link quality for in-vehicle users.

Regarding HO aspects of mIAB, the authors of [97] addressed the problem of group HO of UEs inside buses or trains. They proposed a resource management scheme that contains bandwidth adaptation policy and dynamic bandwidth reservation policy. More specifically, some instants before the moment when a bus or train is expected to arrive at a station, a given amount of resources at the station are reserved for the coming UEs. These resources remain reserved for a predefined interval of time. Simulation results showed that the HO call dropping probability considerably reduced compared to the case where no pre-reservation was performed without much impacting the bandwidth utilization.

The works [95], [96] also investigated the topic of HO in the context of mIAB. The authors of [96] analyzed the system performance of three different scenarios: in the first, there were only macro cells, in the second one there were macro cells and fixed femtocells and in the third one there were macro cells and mobile femtocells deployed in buses. The LTE technology was used for all links. The QoS of cell edge UEs improved after adding fixed and

mobile femtocells. However, mobile UEs enjoyed better performance after adding the mobile femtocells, since these cells could reach areas that fixed femtocells could not. A result comparing the number of HOs considering three different HO strategies (namely, proactive, normal and reactive) was presented. In the presented results, the reactive strategy presented a lower number of HOs compared to the other strategies. However, it was not presented how other metrics were impacted by these three strategies, e.g., link failure rate and UE throughput.

In [95], the authors considered a scenario with MRNs deployed at the top of buses and serving onboard UEs. They provided an analysis of the HO performance and the associated power consumption in LTE. Through computational simulations, the authors compared two cases. The first case was without MRNs deployed on the buses, meaning that all onboard UEs performed their individual HO procedure with macro eNBs. The second case was with MRNs, meaning that only the relays performed the HO procedure to the macro eNBs. Their results showed that the deployment of MRNs reduced the HO rate, the HO failure rate, the ping-pong rate, the UE power consumption and eNB power consumption. Furthermore, the simulation results also showed that UL transmission errors were the most dominant cause of MRNs HO failure. They highlighted that when deploying the relays, the HO procedure played an even more important role in keeping UEs connectivity. With the relays there was a single point of failure, i.e., when the relay HO failed, all UEs connected to the relay were dropped.

B. NON-TERRESTRIAL

In this section we review articles that assume the deployment of non-terrestrial nodes that can both receive and transmit in access and backhaul links. Particularly, we first present works where UAV nodes can be used as mIAB nodes, then, we consider a more general architecture where different types of non-terrestrial nodes, such as High-altitude platforms (HAPs) and satellites, can be deployed as mIAB nodes.

1) UAV

UAV-based MRN will not be part of the 3GPP Release 18 discussions on mIAB, and it is left for future uses in beyond 5G. However, it is still interesting to study its performance from an academic point of view. Compared to the previous types of mobility, e.g., trains and buses, UAVs have important differences. Firstly, in, e.g., buses, the MT and DU are installed outside and inside the buses, respectively, which gives good separation between them, while in UAVs this cannot be accomplished. Besides, UAVs are usually used to serve outside UEs so, for instance, the access links are also moving, but for buses the main purpose is to serve onboard UEs with stationary access links. More precisely, the main use-case for UAVs is coverage extension while for buses is capacity increment. Furthermore, a key point of UAVs is the chance for playing with their height while taking into account their energy consumption and lifetime, which are the main bottleneck for prolonged use of UAVs.

The integration of drones into cellular networks was addressed in [98]. Two different perspectives were presented: 1) how wireless networks can support personal or professional use of drones (called mobile-enabled drones (MEDs)); and 2) how drones can support wireless network performance, i.e., boosting capacity on demand, increasing, coverage range, enhancing reliability and agility as an aerial node called wireless infrastructure drones (WIDs). Regarding WIDs, different possibilities were addressed. One of them was the use of drones as IAB nodes. According to the authors, WIDs alleviate the problem of coverage holes by following the crowd at the cell edge. They highlighted that co-channel interference may be a limiting factor.

In [103], the authors investigated the optimal UAV positioning and the optimal UE-UAV association. Their objective was to maximize the number of UEs served by the UAVs. The formulated problem was subject to a limited peak aggregate rate supported by the wireless backhaul link, a limited bandwidth available for access between UEs and UAV and a UE QoS requirement in terms of maximum path loss that a UE could tolerate before outage. Besides, the UEs could have different priorities to be served by the UAVs. The authors proposed a centralized solution, where for each candidate coordinate of the UAV-BS placement, the problem was transformed into a binary integer linear program, which was then solved through the branch-and-bound method.

In [104], the authors went even further. In order to maximize the overall instantaneous sum-rate, they tried to optimize 3D locations of the UAVs, UE-UAV/gNB association, UE-power allocation and precoder design at backhaul links. It was considered a scenario with macro BS and UAVs. DL was assumed. Aerial UEs received interference from DL signals to other aerial UEs, from gNB to terrestrial UEs, and from backhaul links (gNB to UAVs). UAVs are assumed FD. The following simplifying assumptions were made: ZF canceled out the intra tier interference (perfect CSI) and self-interference was completely eliminated at UAVs. One of the main conclusions of the article was that the performance gains of using UAVs was increased when UEs were distributed in multiple hotspots far from each other in contrast to the case where UEs were in a single hotspot.

In [106], besides UAV placement and UE-UAV association, the authors also investigated resource allocation in an in-band IAB scenario. Orthogonal allocation was considered to avoid interference. Besides, in order to mitigate interference between macro-BSs and UAVs, reverse TDD between them is adopted, e.g., while the macro-BSs are in the DL mode with respect to their serving UEs, UAVs are in UL mode. The number of UL and DL slots are the same. HD is assumed at UAVs. UAVs can be seen as macro UEs. From the ground UEs' point of view, only interference from other UAVs is modeled. More specifically, the authors formulated an optimization problem to maximize the UE utility (log of data rate) subject to fronthaul and backhaul resources

and user assignment. The problem was complex and a sub-optimal approach was adopted. First, it was assumed fixed UAV placement and UE association and then the resource allocation was optimally solved. After that, user association and UAV placement were solved. Results showed the advantage of UAVs in heterogeneous networks (HetNets) and the relevance of the joint optimization considering fronthaul and backhaul constraints.

In [108], [109], [110] the authors added another dimension to the list of optimized parameters of [107]. Besides of optimal UAV 3D positioning, UE-UAV association and resource allocation, they also optimized the UE power allocation. In [108], [109], [110] the drone mounted base stations (DBSs) had in-band FD capabilities, while the UEs were HD capable. The focus was on DL. However, while in [108], the objective was to minimize the number of DBSs while maximizing the overall transmission rate, in [109], [110], the objective was only to maximize the total system throughput. The UEs could be either associated directly to a macro BS or to a DBSs. It was assumed that DBSs could cancel part of their self-interference and due to this the backhaul link of a DBS reused the frequency spectrum of its access link. In [109], simulation results demonstrated gains of deploying DBSs compared to a system without them. In [110], the authors identified, for the considered scenario, a DBS altitude for which DBS position lower than that the path loss was dominated by the NLOS component, and DBS position higher than that the path loss was dominated by the LOS component.

Another use of UAVs was presented in [100]. In that paper, UAVs and ground small cells were deployed to cache[3] content close to the UEs in order to reduce traffic congestion in backhaul. UE association probability for the UAVs and the ground small-cells was derived using stochastic geometry. Besides, the successful content delivery probability was also derived by considering both the intercell and intracell interference. The successful content delivery performance has been improved by 26.6% on average by caching popular content in the UAVs.

2) SATELLITE

The provision of connectivity in remote or unreachable areas such as rural areas is still a problem to be solved by future mobile communications networks. A promising solution to achieve a truly continuous and ubiquitous global connectivity is the employment of space-air-ground integrated networks (SAGIN). With SAGIN, non-terrestrial networks are integrated to terrestrial networks so as to improve coverage, reliability, QoS, spectral efficiency, among others. SAGIN can be considered as a heterogeneous network composed of three sub-networks: a space component composed of, e.g., satellite constellations, an aerial component composed of, e.g., UAVs and HAPs, and a terrestrial component that can include macro and small BSs. Although space and aerial nodes have not been considered as IAB nodes in 3GPP standards yet, these nodes have the capability of providing backhaul links and improving coverage and efficiency of terrestrial networks. In the following, we review some recent works on SAGIN.

Surveys about SAGIN can be found in [111], [112], [113]. Besides presenting SAGIN architecture, [111] classified the articles in physical layer characteristics and spectrum allocation, mobility management, traffic offloading, integrated networks and performance. The focus of [112] was on the use of SAGIN for high speed railways connectivity. Firstly, [112] discussed the current limitations and shortcomings of conventional railway networks such as LTE railway (LTE-R). After that, the authors proposed the integration of railway systems and SAGIN where space- and air-based segments can provide a wide coverage while ground segment can guarantee high throughput. The survey [113] focused on the integration of non-terrestrial networks with 5G and sixth generation (6G) mobile communication systems. According to [113], non-terrestrial networks can act as end users, as relays for backhauling, as relays for end users and as BSs. Furthermore, [113] also highlighted the main challenges of SAGIN that include propagation delay and path loss, coverage, throughput, Doppler effect, mobility management and weather effects.

In [114], SAGIN was considered where UEs are served by small cells and drones while backhaul can be provided by satellites and macro BSs. The formulated problem consisted in finding the optimal user association and resource allocation that maximizes the system's data rate while satisfying QoS requirements. So as to solve the problem, the authors proposed a competitive market solution that can be implemented in a distributed way. A Stackelberg game was formulated in [116] to solve the problem of UE offloading from a terrestrial operator to a satellite operator. A pricing strategy was formulated to incentivize the satellite operator to reserve its own resources to allocate to UEs from terrestrial operators.

In [117], the authors proposed the use of both radio and freespace optical frequencies in SAGIN. Freespace optical enjoys huge bandwidth, lower power consumption and unlicensed spectrum. However, freespace optical suffers from atmospheric turbulence and attenuation due to weather conditions. Motivated by this, the authors proposed an adaptive transmission scheme where RF is used when freespace optical links are with poor channel state. The article [118] focused on physical layer security in SAGIN. The system model assumed that full duplex UAVs are capable of receiving information from Internet of Things (IoT) devices while transmitting artificial noise to the eavesdropping channel. The main objective was to maximize the secure uplink data rate by adapting the information and jamming signal power from UAVs, as well as optimizing the altitude and horizontal position of UAVs.

Machine learning has been applied in SAGIN in the works [115], [119], [120]. In [115], the authors intended

3. The use of cache has not been standardized in 3GPP.

TABLE 1. Entities characteristics.

Parameter	IAB Donor	mIAB node - DU	mIAB node - MT	Pedestrian	Passenger
Height	25 m	2.5 m	3.5 m	1.5 m	1.8 m
Transmit power	35 dBm	24 dBm	24 dBm	24 dBm	24 dBm
Antenna tilt	12°	4°	0°	0°	0°
Antenna array	URA 8 × 8	URA 8 × 8	ULA 64	Single antenna	Single antenna
Antenna element pattern	3GPP 3D [123]	3GPP 3D [123]	Omni	Omni	Omni
Max. antenna element gain	8 dBi	8 dBi	0 dBi	0 dBi	0 dBi
Speed	0 km/h	40 km/h	40 km/h	3 km/h	40 km/h

to maximize the number of transmitted packets by optimizing resource allocation and transmission mode selection. Direct, i.e., UEs transmitting directly to satellites, and cooperative transmission modes, i.e., information signals from UEs are relayed to satellites by aerial nodes such as UAVs, were considered in this work. Motivated by the high complexity of the formulated problem, the authors resorted to reinforcement learning technique by modeling the studied problem as a Markov decision process. In [119], the authors considered SAGIN to complement vehicular networks by improving network capacity and stability of communication links. Several use cases for machine learning applications in SAGIN in vehicular networks were described including mobile edge computing, traffic control, data cache, among others. In [120], a hierarchical structure for processing deep learning tasks in SAGIN was proposed. Motivated by the long transferring distance for collected data and output results from deep learning tasks, the authors proposed a hierarchical methodology where tasks are offloaded from the cloud to different layers of SAGIN based on complexity of deep learning tasks, processing capability of each layer and required QoS.

V. PERFORMANCE EVALUATION

This section presents a performance comparison between a scenario with mIAB and two benchmark scenarios: one with only macro gNBs, called here as *only macros* scenario, and other with macro and pico gNBs fiber-connected to the CN, called here as *macros-picos* scenario. The details concerning the considered simulation modeling are presented in Section V-A and the results are discussed in Section V-B.

A. SIMULATION ASSUMPTIONS

It was considered a simplified version of the Madrid grid [121] as in [122]. As illustrated in Fig. 8, in this scenario, there were nine square blocks, with dimension of 120 m × 120 m. The blocks were surrounded by 3 m wide sidewalks and separated of each other by 14 m wide streets with four lanes, two in each direction. In the central block there were 3 not co-located macro gNBs deployed as in Fig. 8. Pedestrians and buses were randomly placed in the sidewalks and in the streets, respectively. In the intersections, they had a probability of 60 % to continue straight ahead and 40 % to turn left or right with equal probability to each side.

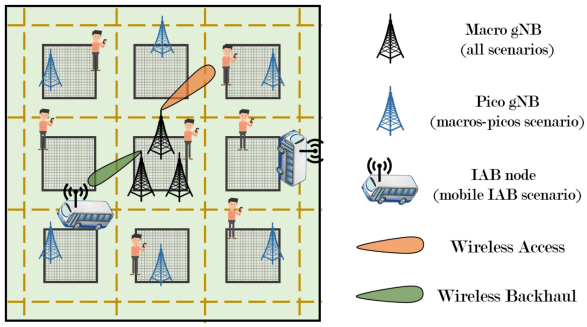

FIGURE 8. Simplified Madrid grid.

The pedestrians walked in the sidewalks and were allowed to cross the roads only in the intersections. Passengers were randomly located inside the buses at any available seat. During the simulation, their position relative to their bus did not change. In the mIAB scenario, mIAB nodes were deployed at the buses. The DU and MT were placed at the back of the buses; however, the DU was inside and the MT was outside at the roof. Important to mention that an mIAB node could not connect to another mIAB node. It could only be served by an IAB donor, i.e., a gNBs. Other parameters related to the entities present in the system, e.g., IAB donors, mIAB nodes, pedestrians and passengers, are presented in Table 1.

The simulations were conducted at 28 GHz with 50 MHz of system bandwidth, standardized in [124, Table 5.3.2-1]. The channel link between the entities present in the simulations was modeled using the 5G-SToRM channel model described in [125], where [125] implements its channel model according to [123]. The adopted channel model from [123], [125] is spatially and time consistent. It considers a distance-dependent path-loss, a lognormal shadowing component and a small-scale fading. Moreover, as illustrated in Fig. 9, all the links with the donor, i.e., donor-pedestrian, donor-MT, donor-DU and donor-passenger, were modeled as urban macro (UMa). All links involving the MT, except the link donor-MT, were modeled as urban micro (UMi), as well as the links DU-pedestrian and pedestrian-passenger. The link DU-passenger was modeled as an indoor hotspot one. The bus body had a penetration loss of 20 dB [123]. Thus, the links with one entity inside the bus and other outside, such as donor-DU, DU-pedestrian, MT-passenger and pedestrian-passenger, suffered this penetration loss. Furthermore, the

TABLE 2. TDD scheme adopted in only macros and macros-picos scenarios.

Slot	1	2	3	4	5	6	7	8	9	10	DL usage	UL usage	Total usage
Macro and Pico gNBs	DL	S (DL)	UL	UL	UL	DL	S (DL)	UL	UL	DL	50%	50%	100%

TABLE 3. TDD scheme adopted in the mIAB scenario.

Slot	1	2	3	4	5	6	7	8	9	10	DL usage	UL usage	Total usage
IAB donor	DL	UL	∅	DL	∅	UL	DL	∅	UL	DL	40%	30%	70%
Backhaul	DL	∅	UL	DL	UL	∅	∅	UL	∅	DL	30%	30%	60%
IAB node	∅	UL	DL	∅	DL	UL	DL	DL	UL	∅	40%	30%	70%

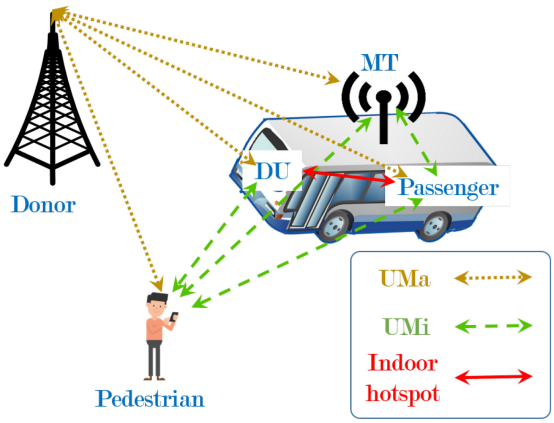

FIGURE 9. Channel types.

link between a DU of a bus and a passenger of another bus suffered twice this penetration loss. Besides, all the links that crossed the bus body were considered NLOS. The other links could be either in LOS or NLOS with a transitional state between them as described in [123].

Regarding resource scheduling, a slot was the minimum scheduling unit. In the time domain, a slot consisted of 14 orthogonal frequency division multiplexing (OFDM) symbols with total time duration of 0.25 ms, while in the frequency domain it consisted of one resource block (RB) with subcarrier spacing of 60 kHz, where one RB corresponded to 12 consecutive subcarriers.

In the frequency domain, the round robin (RR) scheduler was adopted to schedule the RBs. The RR iteratively allocated the RBs, scheduling in a given RB the UE bearer waiting the longest time in the queue. The RR was chosen since it is a well-known scheduler enabling an interested reader to reproduce our performance evaluation. Besides, our main objective was not to find the scheduler that optimizes the system behavior, but rather compare the different solutions under the same conditions, i.e., using the same scheduler. Deep studies about the performance of different scheduling strategies consist in an interesting research topic and is left for further studies.

In the access links, multiple input single output (MISO) transmissions were performed with a matched filter used as precoder. On the other hand, in the backhaul, MIMO transmissions were performed. To take advantage of the multiple antennas at both sides of a backhaul link, the transmission within an RB was multiplexed into streams. For each stream, it was computed a pair of precoder/decoder using the singular value decomposition (SVD) of the channel between an IAB donor and the MT part of an mIAB node. At most the eight streams with the highest singular values were scheduled, subject to having an estimated modulation and coding scheme (MCS) higher than one.

In the time domain, TDD schemes were used to separate transmission and reception of the signals, i.e., in a given slot, data could traverses a link in just one direction, either UL or DL. More specifically, the TDD scheme presented in Table 2 was considered in the only macros and macros-picos scenarios, while the TDD scheme in Table 3 was considered in the IAB scenario, where backhaul UL means that the mIAB MT part transmits data to the IAB donor, while backhaul DL means that the mIAB MT part receives data from the IAB donor. The TDD scheme in Table 2 is standardized by 3GPP in [126], while the one in Table 3 is based on the one proposed in [31] for three hops (in our case we are considering just two hops). Remark that on the one hand, in the scheme of Table 2, macro and pico gNBs are active in 100% of the time, transmitting either in DL or in UL with equal time usage for both DL and UL. On the other hand, in the scheme of Table 3, IAB donor and mIAB node are active only in 70% of the time and with different time usage between DL and UL. One of the reasons for this is the introduction of silence intervals to reduce interference in the system. Specifically regarding the buses, to avoid self-interference, they could not simultaneously receive and transmit data, e.g., receive in the MT while transmitting in the DU.

As a measure of signal strength, the UEs and the mIAB nodes were measuring the reference signal received power (RSRP) of candidate serving cells, where the RSRP is the linear average over the power contributions (in Watts) of the resource elements confined within a SSB transmitted by a candidate serving cell, as defined in [127]. The topology adaptation was based on the highest measured RSRP. The channel quality indicator (CQI)/MCS mapping curves

TABLE 4. Simulation parameters.

Parameter	Value
Layout	Simplified Madrid grid [121], [122]
Carrier frequency	28 GHz
System bandwidth	50 MHz [124, Table 5.3.2-1]
Subcarrier spacing	60 kHz [124, Table 5.3.2-1]
Number of subcarriers per RB	12
Number of RBs	66 [124, Table 5.3.2-1]
Slot duration	0.25 ms
OFDM symbols per slot	14
Channel generation procedure	As described in [123, Fig. 7.6.4-1]
Path loss	Eqs. in [123, Table 7.4.1-1]
Fast fading	As described in [123, Sec.7.5] and [123, Table 7.5-6]
AWGN power per subcarrier	−174 dBm
Noise figure	9 dB
Mobility model	Pedestrian and Vehicular [129]
Number of buses	6
Passengers + pedestrians	72
Percentage of passengers	$\{25\%, 50\%, 75\%\}$
Number of passengers per bus	$\{3, 6, 9\}$
CBR packet size	$\{1024, 2048, 3072\}$ bits
CBR packet inter-arrival time	4 slots

standardized in [128] were used for link adaptation with a target block error rate (BLER) of 10 %. It was also considered an outer loop strategy to avoid the increasing of the BLER. According to this strategy, on the one hand, when a transmission error occurred, the estimated SINR used for the CQI/MCS mapping in the link adaptation was subtracted by a back-off value of 1 dB. On the other hand, when a transmission occurred without error, the estimated SINR had its value added by 0.1 dB.

As previously mentioned, three scenarios were considered. The first with only three macro gNBs deployed at the central block, called here as only macros scenario. The second with the three macro gNBs (acting as IAB donors) plus mIAB nodes deployed in the buses, called here as mIAB scenario. The third with the three macro gNBs plus 6 pico gNBs deployed at the positions indicated in Fig. 8 (at the vertices of a hexagon) called here as macros-picos scenario. In these three scenarios there were 6 buses (as many as pico gNBs) and 72 UEs, i.e., passengers plus pedestrians. The UEs' traffic, in both DL and UL, was modeled as constant bit rate (CBR) flows with packet-inter-arrival time equal to four slots. In the simulations, it was analyzed the impact of the packet size and the impact of the percentage of passengers considering the 72 UEs in the system. For this, nine possible combinations of packet size and percentage of passengers were tested, where the packet size could be equal to 1024, 2048 or 3072 bits and the percentage of passengers considering the 72 UEs in the system could be equal to 25%, 50% or 75% meaning that in each bus there were 3, 6 or 9 passengers. Table 4 summarizes the main simulation parameters.

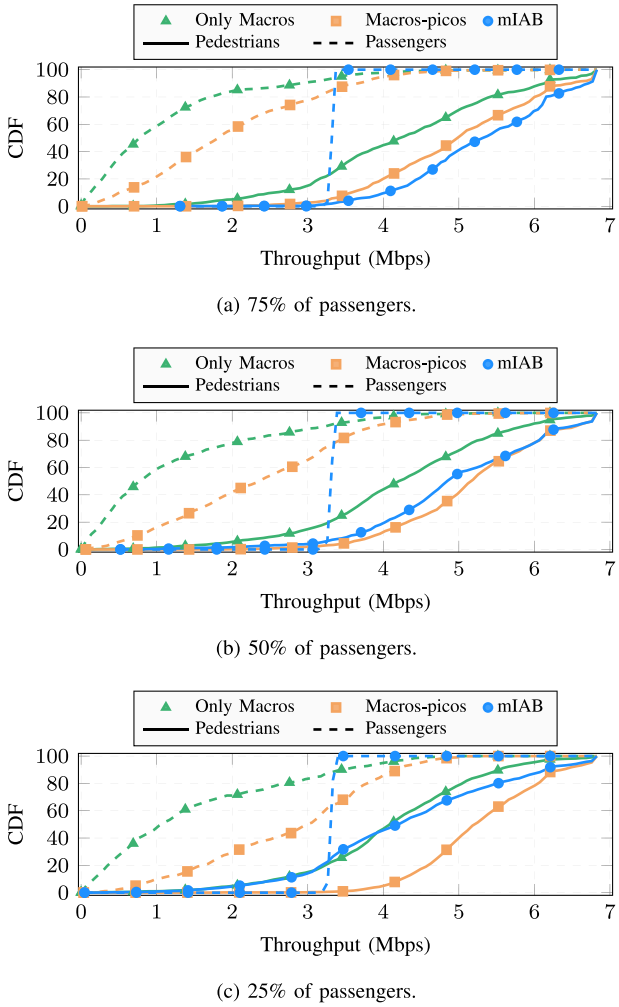

(a) 75% of passengers.

(b) 50% of passengers.

(c) 25% of passengers.

FIGURE 10. Downlink throughput—Impact of percentage of passengers, considering packet size equal to 3072 bits.

In the following, the simulation results are presented. Firstly, we compare the downlink performance of passengers and pedestrians in the three considered scenarios, focusing on their throughput, latency and MCS usage. Secondly, we analyze their performance on the uplink, highlighting the main differences compared to the downlink. Then, we focus on the wireless backhaul quality in the mIAB scenario. Finally, we present the statistics of links served by the IAB donors. More specifically, we analyze the percentage of time that the IAB donors served backhaul and access links.

B. SIMULATION RESULTS

1) DOWNLINK

DOWNLINK THROUGHPUT

Firstly, let's analyze the impact of introducing mIAB on the DL throughput of passengers and pedestrians. Figure 10 presents the DL throughput of passengers (dashed lines) and pedestrians (solid lines) considering a packet size of 3072 bits and for three different percentages of passengers.

First, notice that in the three figures of Fig. 10, the DL throughput of passengers in the mIAB scenario (blue dashed lines with circles as markers) was similar for almost 100% of them. This was due to their vicinity to the mIAB node, i.e., they were next to the DU antennas inside the buses. Besides, compared to the only macros scenario (green dashed lines with triangles as markers), in the mIAB scenario, the DL throughput of the majority of the passengers was remarkably improved. One could argue that in the mIAB scenario there were more gNBs, i.e., the ones in the buses, than in the only macros scenario. However, even when compared to the macros-picos scenario (orange dashed lines with squares as markers), where the number of gNBs was equal to the one in the mIAB scenario, the passenger DL throughput of mIAB scenario was higher than the one for macros-picos scenario in most of the percentiles. Besides, while the DL throughput of all passengers in the mIAB scenario was higher than 3 Mbps, more than half of the passengers in the macros-picos scenario were not able to achieve this throughput. The main reason for this is the fact that signals serving passengers in the only macros and macros-picos scenarios suffered a penetration loss of 20 dB, due to the signal crossing the bus body, while, in the mIAB scenario, the passengers were connected to antennas deployed inside the bus that did not suffer this loss.

Regarding the pedestrians DL throughput in the mIAB scenario, we can see in Fig. 10, that it varied with the percentage of passengers in the system, thus, with the number of pedestrians. Decreasing the percentage of passengers, i.e., increasing the number of pedestrians, their DL throughput decreased. One of the reasons was the adopted fixed IAB TDD scheme, Table 3, which partitioned the slots between backhaul and UEs directly connected to IAB donors without taking into account the real necessity of the system. Thus, it could be better if one adopted a dynamic resource scheduling taking into account the load of backhaul and UEs directly connected to the IAB donors. Besides, compared to the other scenarios, in the IAB scenario, the IAB donors, which served most part of the pedestrians, were active in the DL only in 40% of the time, while in the other scenarios, according to the adopted TDD scheme in Table 2, the macro gNBs were active in the DL during 50% of the time. However, we remark that even if the pedestrians DL throughput decreased in the mIAB scenario compared to the others, it still achieved values high enough to keep a good connectivity.

Figure 11 also presents the DL throughput of passengers (dashed lines) and pedestrians (solid lines), but for three different packet sizes and considering 50% of the UEs in the system as passengers. Similar to the analyses of Fig. 10, we can conclude here that the deployment of mIAB nodes inside the buses improved the passengers DL throughput, while keeping the pedestrians with a good DL throughput. Furthermore, we highlight that for higher percentages of passengers in the system and higher packet size, i.e., more loaded systems, the gains of using mIAB relative to the only macros and macros-picos scenarios were higher.

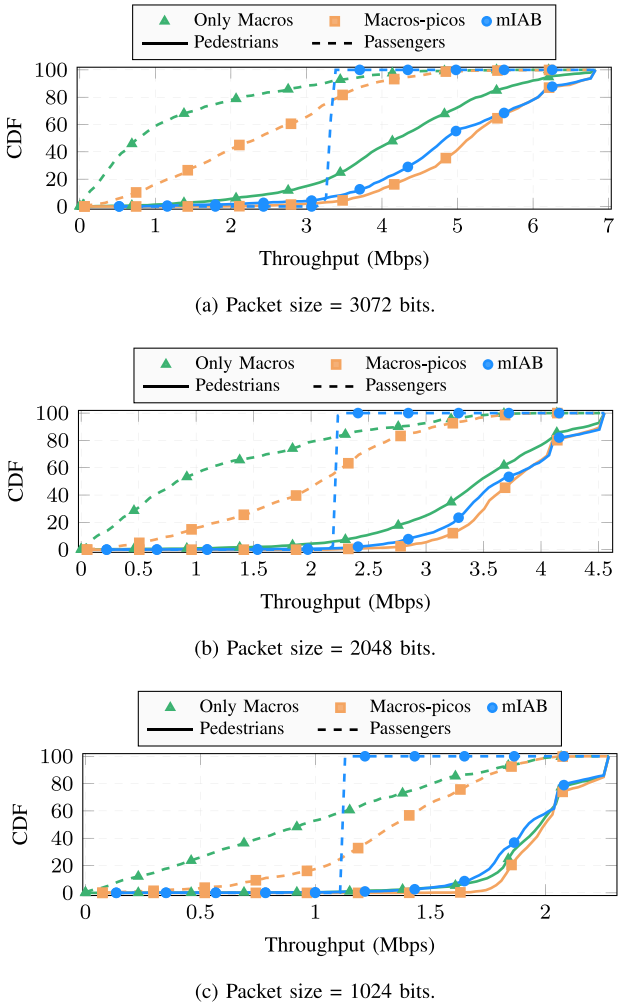

(a) Packet size = 3072 bits.

(b) Packet size = 2048 bits.

(c) Packet size = 1024 bits.

FIGURE 11. Downlink throughput—Impact of packet size, considering percentage of passengers equal to 50%.

DOWNLINK DATA TRANSMISSION QUALITY

Figures 12(a) and 12(b) present the passengers' MCS usage in DL for the only macros and mIAB scenarios, respectively for the configuration with 50% of passengers in the system and packet size of 3072 bits. The red bars represent the percentage of transmissions with error and the blue bars represent the percentage of successful transmissions. First, we remark that Fig. 12(b) does not refer to the passengers end-to-end link quality (IAB donor - passengers), it only refers to the quality of the link between the mIAB nodes and their served passengers. The quality of the link between the IAB donors and the mIAB nodes will be analyzed in Section V-B3.

On the one hand, notice that in Fig. 12(a), in the only macros scenario, the passengers received data mainly with lower MCSs. This was mainly due to the bus penetration loss, which degraded the link between passenger and macro gNBs. Although low MCSs were most frequently used in the transmissions, remark that the sum of NACKs over all MCSs was lower than the target BLER of 10 % adopted in the link

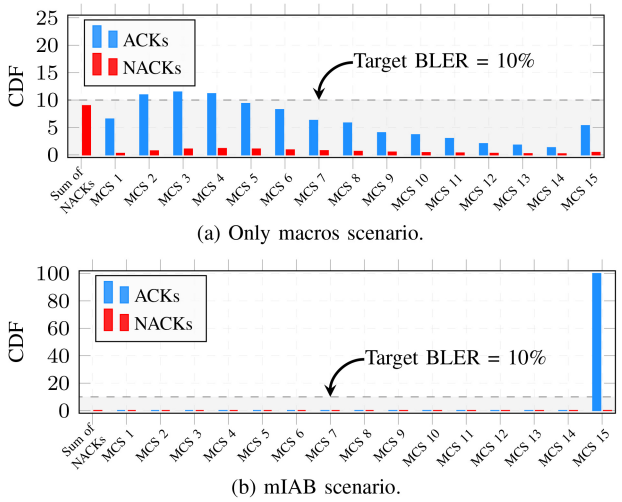

(a) Only macros scenario.

(b) mIAB scenario.

FIGURE 12. Histogram of passengers' MCS usage in DL in a scenario with 50% of passengers and packet size of 3072 bits.

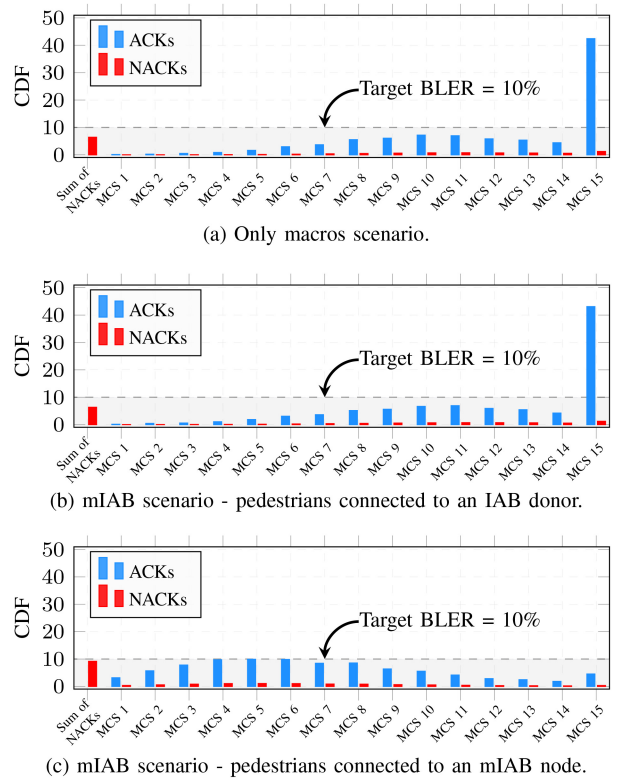

(a) Only macros scenario.

(b) mIAB scenario - pedestrians connected to an IAB donor.

(c) mIAB scenario - pedestrians connected to an mIAB node.

FIGURE 13. Histogram of pedestrians' MCS usage in DL in a scenario with 50% of passengers and packet size of 3072 bits.

adaptation. On the other hand, notice that in Fig. 12(b), in the mIAB scenario, the passengers received data from the mIAB node with the highest MCS and with almost zero transmission error. This is a benefit of deploying the DU part of the mIAB node inside the buses.

The pedestrians' MCS usage in DL is presented in Fig. 13. Figure 13(a) is related to the only macros scenario, while Fig. 13(b) concerns pedestrians connected to an IAB donor

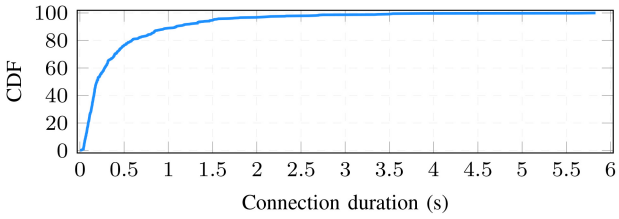

FIGURE 14. CDF of connection duration between a pedestrian and a mIAB node.

in the mIAB scenario and Fig. 13(c) concerns pedestrians connected to an mIAB node also in the mIAB scenario. First, notice that the histograms in Fig. 13(a) and Fig. 13(b) are similar with small differences, meaning that the SINR of a pedestrian connected to a macro gNB in the only macros scenario and the SINR of a pedestrian connected to an IAB donor in the mIAB scenario were similar. Furthermore, considering that the pedestrian signal strength was also similar in both cases, since the macro gNB and the IAB donor had similar characteristics, we conclude that the interference in both cases was also similar.

In the mIAB scenario, 15% of the pedestrians were served by an mIAB node for at least a couple of transmission time intervals (TTIs). Particularly, their connection lasted less than 1 s in 90% of the cases, as illustrated in Fig. 14, which is not good in practice. They connected to a mIAB node due to a higher RSRP. However, when they were receiving data from the DU part of the mIAB node, the MT part was transmitting upstreaming data to the IAB donor in the backhaul, as described in Table 3 slots 3, 5 and 8. Thus, the MT part of the mIAB node caused a high interference to the pedestrians connected to an mIAB node, since both were active at the same time and both were outside the bus, meaning that the interfering link did not suffer attenuation due to the crossing of the bus body. This inference caused low values of SINR and so the usage of low MCSs as shown in Fig. 13(c). Important to remark that this interference was not a problem for the passengers, since they were inside the bus and the signal from the MT part suffered from the bus body penetration loss.

Based on these results, one can conclude that pedestrians should avoid connecting to an mIAB node, unless the signal between them is strong enough to compensate the interference from the MT part and the connection is expected to last longer than a given threshold. For this, one could consider an admission policy to allow a UE to connect to a mIAB cell. The admission criteria could be: a minimum measured RSRP value; a maximum measured interference level (reference signal received quality (RSRQ) instead of RSRP); the relative UE and bus geographical position in a given time interval; etc.

Figures 15(a) and 15(b) present the CDF of SINR and SNR in the DL of pedestrians connected to a macro gNB in the only macros and mIAB scenarios, respectively. Comparing these two figures, notice that the difference between the SINR and SNR curves, i.e., the interference,

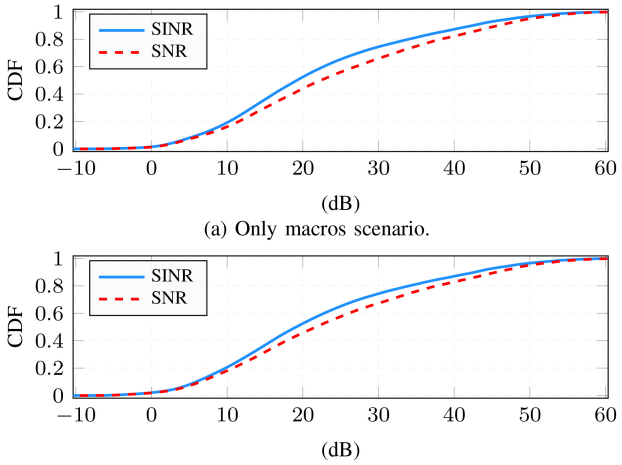

(a) Only macros scenario.

(b) mIAB scenario - pedestrians connected to an IAB donor.

FIGURE 15. SINR and SNR of pedestrians in a scenario with 50% of passengers and packet size of 3072 bits.

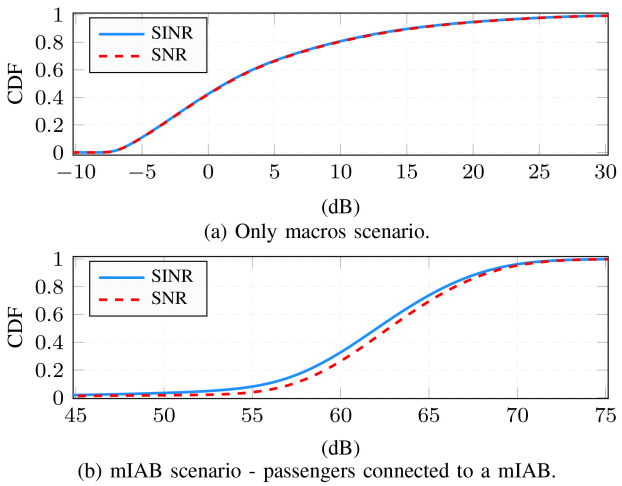

(a) Only macros scenario.

(b) mIAB scenario - passengers connected to a mIAB.

FIGURE 16. SINR and SNR of passengers in a scenario with 50% of passengers and packet size of 3072 bits.

is similar (the difference neither increased nor decreased when changing the scenario). Thus, we can conclude that the deployment of mIAB nodes may not impact the interference that the pedestrians connected to a macro gNB suffer. This is an important result, since the possible dynamic interference caused by mIAB nodes in the UEs served by IAB donors is one of the concerns regarding the deployment of mIAB cells. The interference avoidance was obtained due to the adopted TDD scheme (Table 3), which did not allow transmissions in the access links of mIAB nodes when IAB donors were operating in DL in their access links. The topic of exploiting a TDD scheme for interference handling in mIAB networks is addressed in [130].

Figures 16(a) and 16(b) present the CDF of SINR and SNR in the DL of passengers connected to a macro gNB in the only macros scenario and connected to an mIAB node in the mIAB scenario, respectively. In Fig. 16(a), the SINR and SNR curves are superposed, meaning that in the only

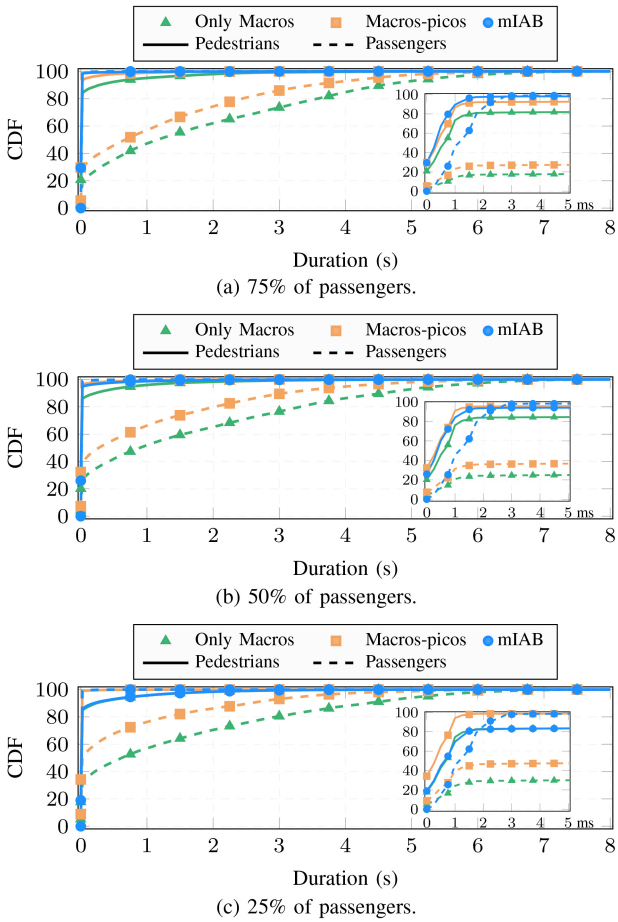

(a) 75% of passengers.

(b) 50% of passengers.

(c) 25% of passengers.

FIGURE 17. Downlink latency—Impact of percentage of passengers, considering packet size equal to 3072 bits.

macros scenario the interference was not a problem for the passengers. This was a consequence of the bus body loss that filtered possible interference links coming from neighbor gNBs. The drawback of the bus body loss is that it filters not only the interference but also the signals serving the passengers, as we can see by the low values of the SNR. In this scenario, 80% the passengers had an SNR lower than 10 dB. On the other hand, in the mIAB scenario, their SNR had a boost when deploying the mIAB nodes in the buses (Fig. 16(b)). In this scenario, when the backhaul (MT part of the mIAB nodes) was operating in the UL, they interfered with the passengers receiving in the DL from the DU part of the mIAB nodes. However, as we can see in Fig. 16(b), the SINR was still high enough to allow transmissions with the highest MCS.

DOWNLINK LATENCY

DL transmissions with low MCS, thus low DL throughput, to the passengers in the only macros and macros-picos scenarios impacted the passengers DL latency as it can be seen in Fig. 17 and Fig. 18. These figures present the CDF of the UEs end-to-end DL latency for different values of the percentage of passengers and of the packet size, respectively.

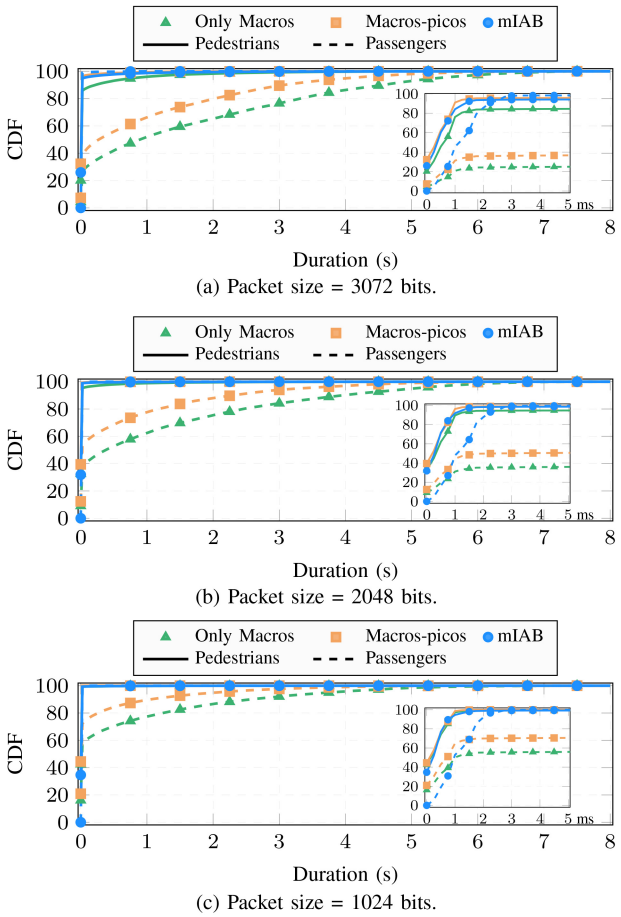

(a) Packet size = 3072 bits.

(b) Packet size = 2048 bits.

(c) Packet size = 1024 bits.

FIGURE 18. Downlink latency—Impact of packet size, considering percentage of passengers equal to 50%.

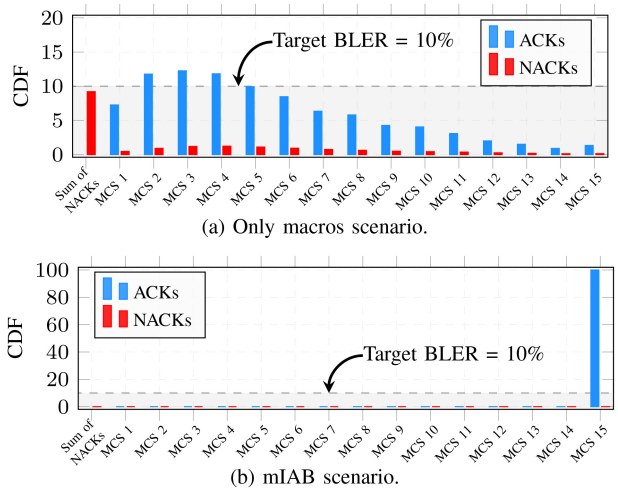

(a) Only macros scenario.

(b) mIAB scenario.

FIGURE 19. Histogram of passengers' MCS usage in UL in a scenario with 50% of passengers and packet size of 3072 bits.

Dashed and solid curves represent the DL latency of passengers and pedestrians, respectively. On the one hand, one can see that passengers using delay sensitive services will suffer in the only macros and macros-picos scenarios, since in the simulations their DL latency achieved values up to 6 s. On the other hand, in the mIAB scenario, DL packet latency was negligible. In that scenario, for the majority of the passengers, in the worst case, the latency was equal to 2 ms. It corresponded to the case where packets were generated in the IAB donor at slot 5 of Table 3 and needed to wait until slot 10 to be transmitted in the backhaul from the IAB donor to the mIAB node and only at the next slot 3 of the next frame it was transmitted from the mIAB node to the passengers, totalizing 8 slots, i.e., 2 ms, of delay. Furthermore, similar to the analyses of DL throughput, we can see that for higher percentages of passengers in the system and higher packet size, i.e., more loaded systems, the gains in the mIAB scenario for the passengers DL latency were higher compared to the other scenarios.

2) UPLINK

Until now, we have analyzed the mIAB performance in the DL. Now, let's focus on the UL. In general, in the UL we came to similar conclusions as the ones drawn in the DL analyses. However, due to different transmit power and interference pattern in DL and UL, some points were different and will be highlighted in the following.

Figure 19 presents the passengers' MCS usage in UL for the only macros and the mIAB scenarios for the configuration with 50% of passengers in the system and packet size of 3072 bits. It is equivalent to Fig. 12, but for the UL. The red bars represent the percentage of transmissions with error and the blue bars represent the percentage of successful transmissions. Comparing Fig. 12(a) and Fig. 19(a), one can notice that in the DL of the only macros scenario, even if the majority of the transmissions were with lower MCSs, 5% of the transmissions were successful with the highest MCS. However, in the UL, less than 1.5% of the transmissions were successful with the highest MCS. The main reason for this was the lower transmit power in the UL compared to the DL. As a consequence, the SINR of the passengers was lower, allowing them to mostly use only the lowest MCSs.

The pedestrians' MCS usage in UL is presented in Fig. 20. Figure 20(a) is related to the only macros scenario, while Fig. 20(b) concerns pedestrians connected to an IAB donor in the mIAB scenario and Fig. 20(c) concerns pedestrians connected to an mIAB node also in the mIAB scenario. Figure 20 is equivalent to Fig. 13, but for the UL. Comparing Fig. 13(c) and Fig. 20(c), one can notice that, for the pedestrians connected to an mIAB node, in the DL, only 5% of the transmissions were successful with the highest MCS, while, in the UL, 13% of the transmissions were successful with the highest MCS. This difference is explained by the fact that, even though the transmit power in the UL was lower, the interference was even lower. More precisely, analyzing Table 3, we can see that a pedestrian connected to an mIAB node receiving data in the DL suffered interference from the MT part of the mIAB node, which was transmitting in the UL to the IAB donor and which did not suffer from

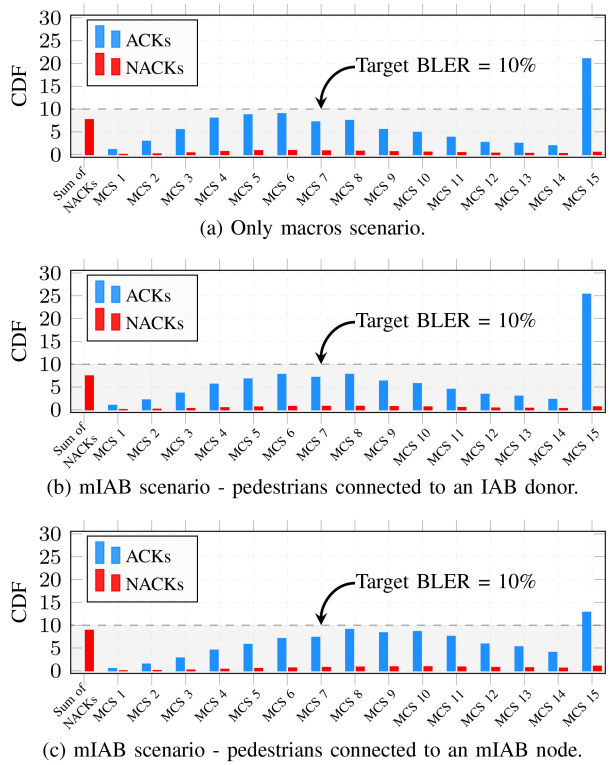

(a) Only macros scenario.

(b) mIAB scenario - pedestrians connected to an IAB donor.

(c) mIAB scenario - pedestrians connected to an mIAB node.

FIGURE 20. Histogram of pedestrians' MCS usage in UL in a scenario with 50% of passengers and packet size of 3072 bits.

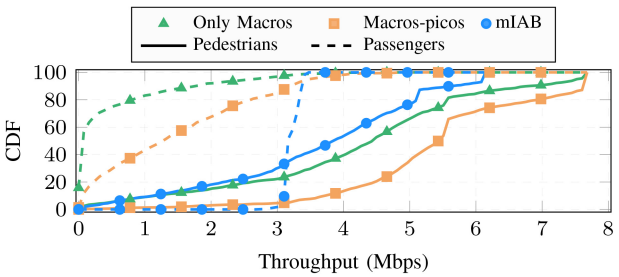

FIGURE 21. Uplink throughput considering packet size equal to 3072 bits and percentage of passengers equal to 50%.

the bus penetration loss since it was placed outside the bus. However, when the same pedestrian was transmitting in the UL to the DU part of an mIAB node, the DU part suffered interference from other pedestrians connected to the IAB donor and transmitting data to it in the upstreaming. Thus, the interference that they caused in the DU also suffered from the bus penetration loss.

The highlighted differences regarding the MCS distribution impacted the UL throughput. Figure 21 presents the UL throughput of passengers (dashed lines) and pedestrians (solid lines) considering packet size equal to 3072 bits and percentage of passengers equal to 50%. It is equivalent to Fig. 10(b), but for the UL. As we have seen, the link quality of passengers in the only macros scenario was worse in the UL than in the DL due to the lower transmit power. As a

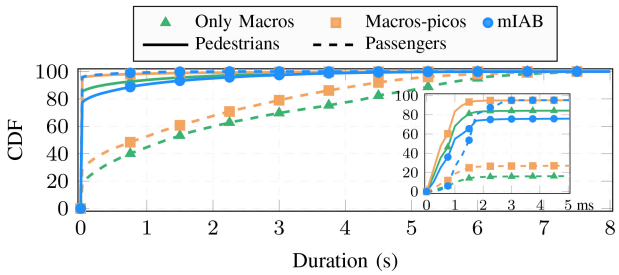

FIGURE 22. Uplink latency considering packet size equal to 3072 bits and percentage of passengers equal to 50%.

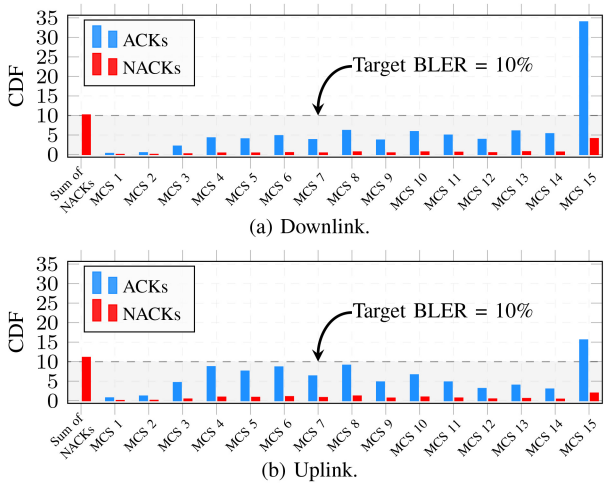

(a) Downlink.

(b) Uplink.

FIGURE 23. Histogram of backhaul's MCS usage in a scenario with 50% of passengers and packet size of 3072 bits.

consequence, in the only macros scenario, passengers UL throughput was worse than their DL throughput, as one can see comparing Fig. 21 and Fig. 10(b). Thus, for the passengers, the gains of deploying mIAB, in terms of throughput, were even higher in the UL. Concerning the pedestrians, in the mIAB scenario, their UL throughput was lower than their corresponding DL throughput. It is explained by the fact that, in the adopted TDD scheme for the mIAB scenario, less time slots are used for UL transmissions than for DL transmissions.

Figure 22 presents the UL latency results. It is equivalent to Fig. 17(b), which presents the DL latency results. Conclusions similar to the ones obtained from the UL throughput can be drawn regarding the UL latency.

3) BACKHAUL QUALITY

In a mIAB scenario, besides the quality of the links of passengers and pedestrians, one should also be careful with the quality of the backhaul link, since when a bus suffered from a bad link to their serving IAB donor, all the passengers connected to it also suffered. Figure 23 presents the histogram of DL and UL backhaul's MCS usage in a scenario with 50% of passengers and packet size of 3072 bits. Comparing Fig. 23(a) and Fig. 23(b) with Fig. 12(a) and Fig. 19(a), respectively, one can again conclude that it was

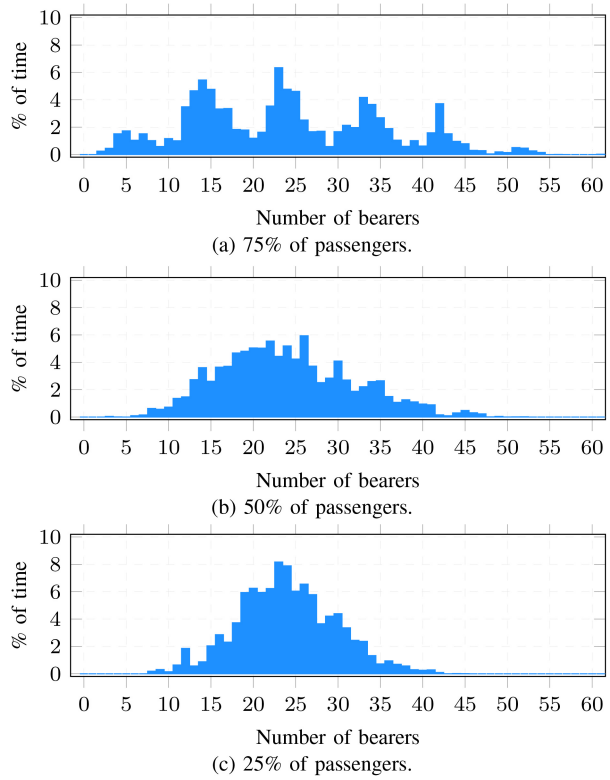

FIGURE 24. Histogram of the number of links served by macro gNBs.

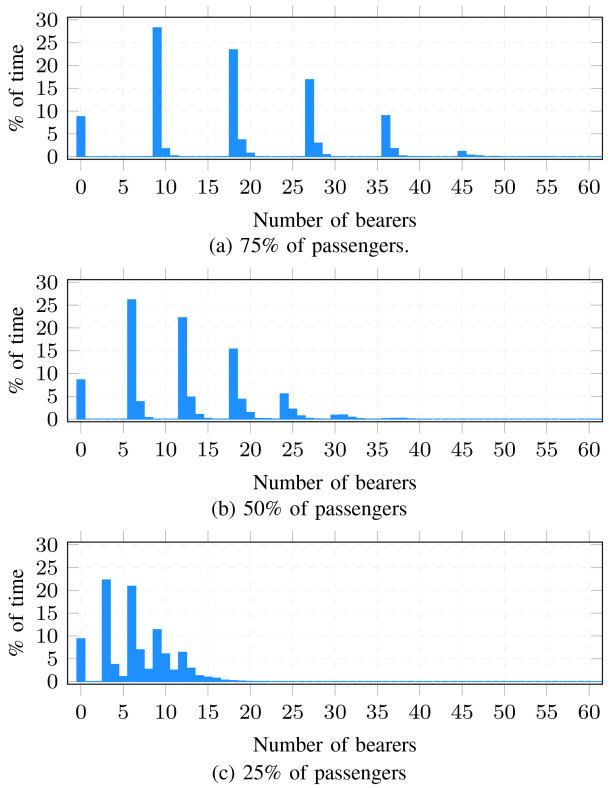

FIGURE 25. Histogram of the number of links in the backhaul served by macro gNBs.

better for a passenger to communicate with the IAB donor through an mIAB node instead of being directly connected to it. The backhaul better link quality was mainly due to the deployment of the mIAB node MT part outside the bus, thus overcoming the bus penetration loss, and also due to the utilization of a uniform linear array (ULA) with 64 antenna elements instead of a single antenna as the passengers did.

4) LINKS SERVED BY IAB DONORS

We have seen that the adopted TDD scheme impacts the results. Thus, it is interesting to try to understand how to better allocate the resources. For this, it is important to understand the profile of the links served by the IAB donors. Hence, in this part we analyze the number of links served by the IAB donors, the percentage of them that are access links and how many links are served by the IAB donors in the backhaul of mIAB nodes.

Figure 24 presents the histogram of the number of links served by IAB donors. When serving a bus, i.e., an mIAB node, an IAB donor indirectly served through the backhaul the UEs served by the bus (almost always, only passengers). Thus, when a bus disconnected from the IAB donor, the load in the donor suddenly changed a lot, since the passengers went away together with the bus. Due to this, as we can see in Fig. 24 the number of links served by an IAB donor could be quite different from one donor to another, since if they served a different number of buses, the difference in the number of served links was approximately multiple of the number of passengers per bus.

This effect is well visible in Fig. 24(a), which refers to the case of 75% of passengers in the system, i.e., nine passengers per bus. Notice that, in this figure, there are six peaks (six was the number of buses in the simulations), each one centered in a multiple of nine, which is the number of passengers in a bus for this case. When the number of passengers was reduced from nine to six and three as in Fig. 24(b) and Fig. 24(c), respectively, the load variability of the IAB donors decreased, since, in those cases, moving a bus from one IAB donor to another did not heavily impact the load of those donors.

Based on these results, one should consider adopting topology adaptation strategies that take into account the IAB donor load. This may avoid overloading IAB donors when changing the serving donor of a given bus.

Figure 25 focuses only on the number of backhaul links served by IAB donors and presents the histogram of this number. Since, in the backhaul, the IAB donors were serving links from the buses, one could expect that through the backhaul the donors would serve a number of links multiple of the number of passengers in the buses. However, Fig. 25 shows that sometimes the backhaul served a number of links a little bit higher than a number multiple of the number of passengers per bus. For example, in Fig. 25(a), which refers to the case of 75% of passengers in the system, i.e., nine passengers per bus, there are six peaks, each one in multiples of nine, plus some bars corresponding to numbers a little bit higher that the closest multiple of nine. This is explained by

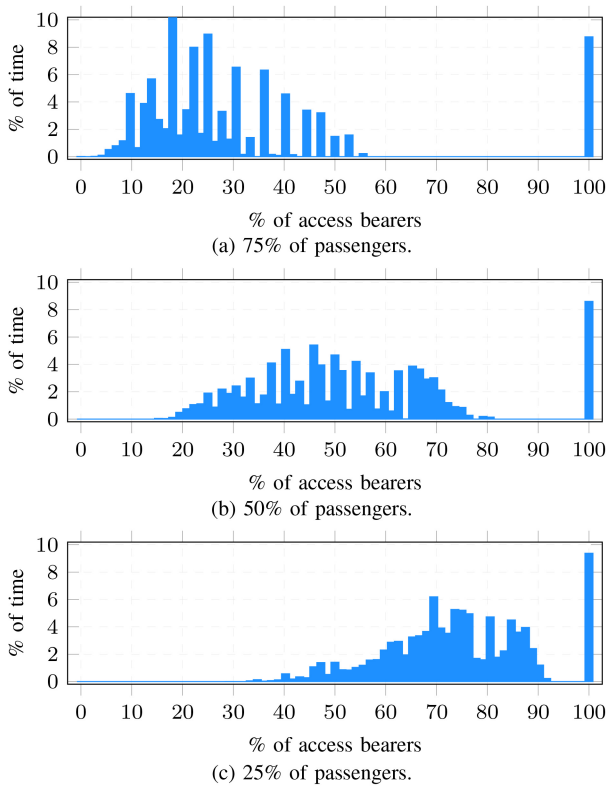

FIGURE 26. Histogram of the percentage of links served by the macro gNBs that are access links.

the fact that buses could serve not only passengers, but also pedestrians, totalizing a number of served links equal to the number of passengers plus a small number of pedestrians.

Finally, Fig. 26 presents the histograms of the percentage of links served by the IAB donors that correspond to access links. The complementary of these numbers corresponds to backhaul links. Remark that the percentage of links that are access links varies a lot. As a consequence, one can conclude that adopting fixed time/frequency resources multiplexing schemes between donors and nodes may waste resources. For example, when the percentage of access links served by the IAB donor was low, it could be better to schedule more resources to the backhaul of connected mIAB nodes. In other words, one should consider adopting dynamic time/frequency resource multiplexing between access and backhaul based on the type of served links.

Based on the conclusions drawn in this section and on the concepts presented until now, next section summarizes the main learned lessons and points out open issues and possible directions to address them.

VI. LESSONS LEARNED, OPEN ISSUES AND FUTURE DIRECTIONS

The high-data rate and huge bandwidth requirements of future networks, e.g., 5G-Advanced and 6G, are a strong motivation to explore mmWave and even higher frequencies, e.g., Sub-Terahertz (Sub-THz). Networks working in such frequencies are expected to be even denser compared to 4G and 5G. This makes the study of IAB and other solutions that overcome the need of wired connected nodes, e.g., network controlled repeater (NCR) and reconfigurable intelligent surface (RIS) based solutions, still important. In this context, wireless backhaul as an enabler of future networks at the infrastructure level makes mIAB a potential 6G application to achieve the key 6G requirements, as also mentioned in [131]. Specially, while the industrial needs for IAB on the trains/buses may increase, it is expected that 6G focuses on more advanced mIAB setups such as mIAB on the drones for, e.g., public safety applications, or mIAB on the satellites/LEOs for uninterrupted coverage. Thus, in the following, we present the main learned lessons and point out open issues as well as possible directions to address them.

A. CELL PLANNING

The mIAB state-of-the-art works which consider transports with previously known behavior, e.g., trains and buses, usually take advantage of that and deploy IAB donors in strategic places, e.g., along the railway track. For systems without a well-defined behavior, e.g., vehicles moving in a city, it is more challenging to design the system in advance, e.g., to define where the IAB donors should be deployed and how resource allocation and interference management can be handled. A promising direction is to adopt artificial intelligence (AI)-based solutions to learn possible mIAB node trajectories and how the traffic varies along the day in order to be able to deploy IAB donors in strategic positions.

B. MOBILITY MANAGEMENT

A challenge imposed by the mobility of an mIAB node is that it can suddenly overload its target IAB donor if the donor is not prepared to receive this new mIAB node. Similar to the previous topic, one adopted approach to deal with the mobility of mIAB nodes is to exploit the knowledge of the transport position and its trajectory, e.g., where a train or bus is and when they are going to arrive at the station. It allows the system to configure in advance the next IAB donor to receive the incoming UEs. However, this strategy is more challenging when we deal with vehicles without a well-defined trajectory. A promising solution to investigate is also to use prediction-based methods in those cases. For example, if the system is able to predict the arrival of an mIAB node, and its corresponding additional traffic, instants before it arrives, nearby BSs can perform load balancing in advance in order to reserve resources for the coming node.

C. DYNAMIC INTERFERENCE MANAGEMENT

Whether interference management is required or not depends on different parameters such as the mIAB transmit power, scheduling, power adaptation capability of the nodes, etc. Many works considered the access link provided by mIAB nodes deployed in a frequency spectrum different from the one used by the rest of the system in order to eliminate the interference caused by the mobility of those

UEs through the system. This is not an efficient solution since the spectrum is expensive and scarce and might stay unused in a given area as long as no mIAB node is there. On the other hand, it is still a challenge to deploy access and backhaul links at the same frequency band due to the dynamic interference caused by the mobility of the mIAB nodes. Thus, solutions for in-band interference management must be further investigated. For example, one can perform power control in the mIAB nodes access links in order to reduce/avoid interfering with nearby UEs connected to the IAB donor. Another option is to insert slots of silence on the TDD frame pattern, as investigated in [130].

D. BANDWIDTH ALLOCATION FOR ACCESS AND BACKHAUL

Most of the works considering in-band deployment of mIAB adopted a fixed split of the resources (either in frequency or in time) between access and backhaul links. A strategy for sharing resources between backhaul link and access links of inside and outside UEs is still a challenge and must be further investigated, since it can lead to more efficient use of the spectrum. For example, dynamic spectrum partitioning could be performed taking into account the data load to be transmitted in the backhaul and in the access links of IAB donor and mIAB nodes. This solution guarantees fairness and avoids the waste of resources in case part of the spectrum is reserved for a given type of link, e.g., backhaul, but there is not enough data to be transmitted in that link.

E. ANTENNA DEPLOYMENT

It is almost a consensus that at least for trains and buses antennas are going to be deployed outside and at the top of these transports being connected to inside APs which will provide connectivity for inside UEs. However, practical considerations must still be further evaluated, e.g., each operator will need to deploy its own equipment or will the infrastructure be shared, e.g., computational resources, antennas and frequency spectrum. Moreover, since a possible use case of mIAB nodes is to serve not only onboard UEs but also surrounding UEs, it is important to evaluate and compare pros and cons of deploying DU antennas either only inside or both inside and outside of mIAB nodes.

F. ROLE OF UAV

UAV-based communication is not considered in 3GPP Release 18 work-item on mIAB. However, from an academic perspective, it is still interesting to investigate its performance. Works which use UAVs to enhance the coverage of the network usually first define an optimal position for the UAVs and fix them there. It is still under evaluation how UAVs perform when continually moving either to provide access link for UEs or to provide a wireless backhaul for other IABs nodes.

G. IMPROVED RELIABILITY FOR C-PLANE

3GPP standard documents do not yet cover mIAB aspects. Different aspects should still be investigated, e.g., the possibility of splitting user and control planes as in dual connectivity (DC) scenarios. In the context of mIAB U-plane could be multi-hop while C-plane would be one-hop [132]. This approach aims at reducing latency and failure probability. Furthermore, U/C-planes could even be deployed at different frequencies, where U-plane would be deployed at mmWave for enhanced throughput while C-plane would be deployed at C-band for higher reliability and coverage.

H. TOPOLOGY ADAPTATION ON MOBILE IAB

With inter-CU topology adaptation, an IAB node migrates from an old parent to a new parent where both parent nodes are served by different IAB donor CUs. The current discussions are about the need for both MT and DU parts of the migrating IAB node to handover. The main point is that DU migration requires that all child nodes and UEs should perform HO to the new target donor-CU. This is not the case when only MT-part HO is executed. DU migration involves context transfer of the child IAB nodes and UEs, update of their security keys and causes a large amount of signaling to be exchanged via the Xn, F1 and radio interfaces [133]. This flood of signaling is called signaling storm. The main concern is that this procedure may cause service interruption as, currently, each DU can be connected simultaneously to only one CU. One of the envisaged solutions is the possibility of the support of two logical DUs, but this may increase the complexity of IAB. Although these discussions on 3GPP are focused on fixed IAB, they certainly are of utmost relevance for future discussions on mIAB where topology adaptation should be more frequent.

I. SIGNALING OPTIMIZATION FOR GROUP HO

Another important aspect that has been discussed on 3GPP meetings is about the optimization of group HO when the DU part changes its parent in inter-CU topology adaptation. If standard HO procedure is followed, all child nodes and UEs would perform Xn HO procedure including the random access (RACH) procedure. However, note that the RACH procedure is not necessary in these cases since there is no change in the UE‘s strongest cell and child IAB nodes’ strongest parent. Finally, group signaling could be tailored for this case where HO messages of several UEs could be concatenated/compressed [134]. As an example, each UE‘s RRC reconfiguration message could be significantly reduced by updating only few parameters.

VII. CONCLUSION

As presented in this work, mIAB is a candidate solution to address at least two challenges of current networks. Firstly, it enhances the service of moving UEs, e.g., passengers of trains and buses, guaranteeing that they are always connected and avoiding overloading the network with HO messages

when a group of moving UEs enters simultaneously the coverage area of a new cell. Secondly, it allows a quick deployment of new cells to provide/improve connectivity in high demanding areas with the deployment of mIAB nodes.

The basis for the deployment of mIAB were presented. They are: current status of IAB standardization in 5G NR and state-of-the-art works regarding fixed IAB and mIAB. In order to help readers interested in this subject, the state-of-the-art works were classified following different criteria. On the one hand, fixed IAB related works were classified according to the studied dimensions, system modeling assumptions/constraints, considered problem objectives and KPIs, solution approaches and adopted mathematical tools. On the other hand, mIAB related works were grouped according to the type of mobile node, e.g., train, bus, UAV, etc. It was noticed that works considering similar mobile nodes usually consider similar problems, e.g., UAV positioning, and take advantage of specific characteristics of each mobile node, e.g., known trajectory of buses.

After the literature review, we have performed an extensive analysis of mIAB based on computational simulations. It was considered an urban macro scenario where IAB nodes were deployed in buses in order to improve the passengers' connection. It was presented passengers and pedestrians throughput, latency and link quality in both downlink and uplink transmission directions. Results related to the wireless backhaul were also presented as well as the profile of links served by the IAB donors. It was concluded that the deployment of the DU part of an IAB node inside a bus and its MT part outside the bus remarkably improves the passengers throughput and latency. This is due to the fact that this deployment overcomes the significant bus penetration loss that a link between a BS outside the bus and a passenger suffers. Moreover, it was also concluded that an admission policy to allow a UE to connect to a mIAB cell should be adopted. The admission criteria could be: a minimum measured RSRP value; a maximum measured interference level (RSRQ instead of RSRP); the relative UE and bus geographical position in a given time interval; etc. Furthermore, it was concluded that the adopted topology adaptation and TDD scheme play an important role directly impacting the interference management strategy. Thus, it would be better if dynamic topology adaptation and time/frequency resource scheduling were adopted taking into account the IAB donor load, e.g., amount of served traffic from access and backhaul links.

Finally, we have summarized lessons learned, open issues and future directions related to mIAB. One important challenge is how to deal with the dynamic interference caused by mobile cells when moving around the system, specially in the case with in-band deployment of backhaul and access. Besides, a promising solution for this and other challenges is the use of predictive solutions, e.g., AI-based, in order to anticipate what is going to happen and prepare the system in advance.

REFERENCES

[1] V. Jungnickel et al., "The role of small cells, coordinated multipoint, and massive MIMO in 5G," *IEEE Commun. Mag.*, vol. 52, no. 5, pp. 44–51, May 2014, doi: 10.1109/MCOM.2014.6815892.

[2] S. Dang, O. Amin, B. Shihada, and M.-S. Alouini, "What should 6G be?" *Nat. Electron.*, vol. 3, pp. 20–29, Jan. 2020, doi: 10.1038/s41928-019-0355-6.

[3] T. Inoue, "5G NR release 16 and millimeter wave integrated access and backhaul," in *Proc. IEEE Radio Wireless Symp. (RWS)*, San Antonio, TX, USA, Jan. 2020, pp. 56–59, doi: 10.1109/RWS45077.2020.9050108.

[4] W. Ni and I. B. Collings, "A new adaptive frequency allocation algorithm in multi-hop point-to-point FDD backhaul networks for metro cells," in *Proc. Int. Symp. Commun. Inf. Technol. (ISCIT)*, Gold Coast, QLD, Australia, Oct. 2012, pp. 187–192, doi: 10.1109/ISCIT.2012.6380887.

[5] H. S. Dhillon and G. Caire, "Scalability of line-of-sight massive MIMO mesh networks for wireless backhaul," in *Proc. IEEE Int. Symp. Inf. Theory*, Honolulu, HI, USA, Jun. 2014, pp. 2709–2713, doi: 10.1109/ISIT.2014.6875326.

[6] D. Schulz et al., "Optical wireless LED link for the backhaul of small cells," in *Proc. Opt. Fiber Commun. Conf. Exhibit. (OFC)*, Los Angeles, CA, USA, Mar. 2015, pp. 1–3, doi: 10.1364/OFC.2015.M2F.8.

[7] T. F. Rahman, C. Sacchi, and C. Stallo, "mm-Wave LTE-A small-cell wireless backhauling based on TH-IR techniques," in *Proc. IEEE Aerosp. Conf.*, Big Sky, MT, USA, Mar. 2015, pp. 1–9, doi: 10.1109/AERO.2015.7118906.

[8] B. Yin, N. Wang, Y. Fan, X. Sun, D. He, and W. Liu, "Evaluation of TDM-based integrated access and backhaul schemes for 5G and beyond at mmWave band," in *Proc. Int. Conf. Cyber-Enabled Distrib. Comput. Knowl. Discov. (CyberC)*, Chongqing, China, Oct. 2020, pp. 348–353, doi: 10.1109/CyberC49757.2020.00065.

[9] W. Xi, N.-T. Mao, and K. Rundberget, "Cost comparisons of backhaul transport technologies for 5G fixed wireless access," in *Proc. IEEE 5G World Forum (5GWF)*, Santa Clara, CA, USA, Jul. 2018, pp. 159–163, doi: 10.1109/5GWF.2018.8516977.

[10] Y. Zhang, M. A. Kishk, and M.-S. Alouini, "A survey on integrated access and backhaul networks," *Front. Commun. Netw.*, vol. 2, pp. 1–24, Jun. 2021, doi: 10.3389/frcmn.2021.647284.

[11] S. Jaffry, R. Hussain, X. Gui, and S. F. Hasan, "A comprehensive survey on moving networks," *IEEE Commun. Surveys Tuts.*, vol. 23, no. 1, pp. 110–136, 1st Quart., 2021, doi: 10.1109/COMST.2020.3029005.

[12] "Overview of 3GPP release 10," 3rd Gener. Partnership Project (3GPP), Sophia Antipolis, France, Rep. TR, Jul. 2014. [Online]. Available: https://www.3gpp.org/ftp/Information/WORK_PLAN/Description_Releases/

[13] "Evolved universal terrestrial radio access (E-UTRA); relay architectures for E-UTRA (LTE-Advanced)," 3rd Gener. Partnership Project (3GPP), Sophia Antipolis, France, Rep. TR 36.806, Apr. 2010. [Online]. Available: http://www.3gpp.org/ftp/Specs/html-info/36806.htm

[14] M. Polese et al., "Integrated access and backhaul in 5G mmWave networks: Potential and challenges," *IEEE Commun. Mag.*, vol. 58, no. 3, pp. 62–68, Mar. 2020, doi: 10.1109/MCOM.001.1900346.

[15] "NR; study on integrated access and backhaul (release 16), v.16.0.0," 3rd Gener. Partnership Project (3GPP), Sophia Antipolis, France, 3GPP Rep. TR 38.874, Dec. 2018. [Online]. Available: http://www.3gpp.org/ftp/Specs/html-info/38874.htm

[16] *NR; NR and NG-RAN Overall Description; Stage 2, V.16.3.0*, 3GPP Standard TS 38.300, Sep. 2020. [Online]. Available: http://www.3gpp.org/ftp/Specs/html-info/38300.htm

[17] *NR; Integrated Access and Backhaul Radio Transmission and Reception, V.16.1.0*, 3GPP Standard TS 38.174, Dec. 2020. [Online]. Available: http://www.3gpp.org/ftp/Specs/html-info/38174.htm

[18] C. Madapatha et al., "On integrated access and backhaul networks: Current status and potentials," *IEEE Open J. Commu. Soc.*, vol. 1, pp. 1374–1389, 2020, doi: 10.1109/OJCOMS.2020.3022529.

[19] *NG-RAN; F1 General Aspects and Principles (Release 16), V.16.4.0*, 3GPP Standard TS 38.470, Apr. 2021. [Online]. Available: https://www.3gpp.org/ftp/Specs/archive/38_series/38.470/38470-g40.zip

[20] *NR; Backhaul Adaptation Protocol (BAP) Specification (Release 16), V.16.4.0*, 3GPP Standard TS 38.340, Mar. 2021. [Online]. Available: http://www.3gpp.org/ftp/Specs/html-info/38340.htm

[21] *NG-RAN; Architecture Description, V.16.3.0*, 3GPP Standard TS 38.401, Sep. 2020. [Online]. Available: http://www.3gpp.org/ftp/Specs/html-info/383401.htm

[22] E. Dhalman, S. Parkvall, and J. Skold, *5G NR: The Next Generation Wireless Access Technology*, M. Conner, Ed. Amsterdam, The Netherlands: Academic, 2021.

[23] "New WID on enhancements to integrated access and backhaul," 3rd Gener. Partnership Project (3GPP), Sophia Antipolis, France, document RP 210758, meeting no. 91e, Mar. 2021. [Online]. Available: https://www.3gpp.org/tp/TSG_RAN/TSG_RAN/TSGR_91e/DocsRP-210758.zip

[24] E. Dhalman, S. Parkvall, and J. Skold, *5G NR The Next Generation Wireless Access Technology*, 2nd ed. M. Conner, Ed. Amsterdam, The Netherlands: Academic, 2021.

[25] O. Teyeb, A. Muhammad, G. Mildh, E. Dahlman, F. Barac, and B. Makki, "Integrated access backhauled networks," in *Proc. IEEE Veh. Technol. Conf. (VTC)*, Honolulu, HI, USA, Nov. 2019, pp. 1–5, doi: 10.1109/VTCFall.2019.8891507.

[26] T. Tian et al., "Field trial on millimeter wave integrated access and backhaul," in *Proc. IEEE Veh. Technol. Conf. (VTC)*, Kuala Lumpur, Malaysia, Apr. 2019, pp. 1–5, doi: 10.1109/VTCSpring.2019.8746375.

[27] H. Ronkainen, J. Edstam, A. Ericsson, and C. Östberg, "Integrated access and backhaul: A new type of wireless backhaul in 5G," *Front. Commun. Netw.*, vol. 2, Apr. 2021, Art. no. 636949, doi: 10.3389/frcmn.2021.636949.

[28] C. Madapatha, B. Makki, A. Muhammad, E. Dahlman, M.-S. Alouini, and T. Svensson, "On topology optimization and routing in integrated access and backhaul networks: A genetic algorithm-based approach," *IEEE Open J. Commun. Soc.*, vol. 2, pp. 2273–2291, 2021, doi: 10.1109/OJCOMS.2021.3114669.

[29] M. Cudak, A. Ghosh, A. Ghosh, and J. Andrews, "Integrated access and backhaul: A key enabler for 5G millimeter-wave deployments," *IEEE Commun. Mag.*, vol. 59, no. 4, pp. 88–94, Apr. 2021, doi: 10.1109/MCOM.001.2000690.

[30] J. Zhang, N. Garg, M. Holm, and T. Ratnarajah, "Design of full duplex millimeter-wave integrated access and backhaul networks," *IEEE Wireless Commun.*, vol. 28, no. 1, pp. 60–67, Feb. 2021, doi: 10.1109/MWC.001.2000199.

[31] H. Ronkainen, J. Edstam, A. Ericsson, and C. Östberg. "Integrated access and backhaul—A new type of wireless backhaul in 5G." Jun. 2020. [Online]. Available: https://www.ericsson.com/en/reports-and-papers/ericsson-technology-review/articles/introducing-integrated-access-and-backhaul

[32] M. N. Islam, N. Abedini, G. Hampel, S. Subramanian, and J. Li, "Investigation of performance in integrated access and backhaul networks," in *Proc. IEEE Conf. Comput. Commun. (INFOCOM)*, Honolulu, HI, USA, Jul. 2018, pp. 597–602, doi: 10.1109/INFCOMW.2018.8406872.

[33] M. Polese, M. Giordani, A. Roy, S. Goyal, D. Castor, and M. Zorzi, "End-to-end simulation of integrated access and backhaul at mmWaves," in *Proc. IEEE Int. Workshop Comput.-Aided Model. Des. Commun. Links Netw. (CAMAD)*, Barcelona, Spain, Nov. 2018, pp. 1–7, doi: 10.1109/CAMAD.2018.8514996.

[34] C. Saha and H. S. Dhillon, "Millimeter wave integrated access and backhaul in 5G: Performance analysis and design insights," *IEEE J. Sel. Areas Commun.*, vol. 37, no. 12, pp. 2669–2684, Dec. 2019, doi: 10.1109/JSAC.2019.2947997.

[35] S. Ranjan, P. Chaporkar, P. Jha, and A. Karandikar, "Backhaul-aware cell selection policies in 5G IAB networks," in *Proc. IEEE Wireless Commun. Netw. Conf. (WCNC)*, Nanjing, China, May 2021, pp. 1–6, doi: 10.1109/WCNC49053.2021.9417398.

[36] M. Polese, M. Giordani, A. Roy, D. Castor, and M. Zorzi, "Distributed path selection strategies for integrated access and backhaul at mmWaves," in *Proc. IEEE Global Telecommun. Conf. (GLOBECOM)*, Abu Dhabi, UAE, Dec. 2018, pp. 1–7, doi: 10.1109/GLOCOM.2018.8647977.

[37] M. E. Rasekh, D. Guo, and U. Madhow, "Joint routing and resource allocation for millimeter wave picocellular backhaul," *IEEE Trans. Wireless Commun.*, vol. 19, no. 2, pp. 783–794, Feb. 2020, doi: 10.1109/TWC.2019.2948624.

[38] M. E. Rasekh, D. Guo, and U. Madhow, "Interference-aware routing and spectrum allocation for millimeter wave backhaul in urban picocells," in *Proc. Allerton Conf. Commun. Control Comput. (Allerton)*, Monticello, IL, USA, Sep. 2015, pp. 1–7, doi: 10.1109/ALLERTON.2015.7557347.

[39] E. Arribas et al., "Optimizing mmWave wireless backhaul scheduling," *IEEE Trans. Mobile Comput.*, vol. 19, no. 10, pp. 2409–2428, Oct. 2020, doi: 10.1109/TMC.2019.2924884.

[40] M. Simsek, M. Narasimha, O. Orhan, H. Nikopour, W. Mao, and S. Talwar, "Optimal topology formation and adaptation of integrated access and backhaul networks," *Front. Commun. Netw.*, vol. 1, pp. 1–12, Jan. 2021, doi: 10.3389/frcmn.2020.608088.

[41] T. K. Vu, M. Bennis, M. Debbah, and M. Latva-Aho, "Joint path selection and rate allocation framework for 5G self-backhauled mm-wave networks," *IEEE Trans. Wireless Commun.*, vol. 18, no. 4, pp. 2431–2445, Apr. 2019, doi: 10.1109/TWC.2019.2904275.

[42] Y. Li, J. Luo, R. A. Stirling-Gallacher, and G. Caire, "Integrated access and backhaul optimization for millimeter wave heterogeneous networks," Jan. 2019, *arXiv:1901.04959*.

[43] A. HasanzadeZonuzy, I.-H. Hou, and S. Shakkottai, "Broadcasting real-time flows in integrated backhaul and access 5G networks," in *Proc. Int. Symp. Model. Opt. Mobile Ad Hoc Wireless Netw. (WiOPT)*, Avignon, France, Jul. 2019, pp. 1–8, doi: 10.23919/WiOPT47501.2019.9144141.

[44] B. Zhai, M. Yu, A. Tang, and X. Wang, "Mesh architecture for efficient integrated access and backhaul networking," in *Proc. IEEE Wireless Commun. Netw. Conf. (WCNC)*, Seoul, South Korea, May 2020, pp. 1–6, doi: 10.1109/WCNC45663.2020.9120546.

[45] Q. Zhang, K. Luo, W. Wang, and T. Jiang, "Joint C-OMA and C-NOMA wireless backhaul scheduling in heterogeneous ultra dense networks," *IEEE Trans. Wireless Commun.*, vol. 19, no. 2, pp. 874–887, Feb. 2020, doi: 10.1109/TWC.2019.2949791.

[46] J. Y. Lai, W.-H. Wu, and Y. T. Su, "Resource allocation and node placement in multi-hop heterogeneous integrated-access-and-backhaul networks," *IEEE Access*, vol. 8, pp. 122937–122958, 2020, doi: 10.1109/ACCESS.2020.3007501.

[47] M. A. Al-Jarrah, E. Alsusa, A. Al-Dweik, and M.-S. Alouini, "Performance analysis of wireless mesh backhauling using intelligent reflecting surfaces," *IEEE Trans. Wireless Commun.*, vol. 20, no. 6, pp. 3597–3610, Jun. 2021, doi: 10.1109/TWC.2021.3052370.

[48] C. Fang, C. Madapatha, B. Makki, and T. Svensson, "Joint scheduling and throughput maximization in self-backhauled millimeter wave cellular networks," in *Proc. Int. Symp. Wireless Commun. Syst. (ISWCS)*, Berlin, Germany, Sep. 2021, pp. 1–6, doi: 10.1109/ISWCS49558.2021.9562232.

[49] H. Alghafari and M. S. Haghighi, "Decentralized joint resource allocation and path selection in multi-hop integrated access backhaul 5G networks," *Comput. Netw.*, vol. 207, Apr. 2022, Art. no. 108837.

[50] C. Madapatha, B. Makki, H. Guo, and T. Svensson, "Constrained deployment optimization in integrated access and backhaul networks," Oct. 2022, *arXiv:2210.05253*.

[51] C. Saha, M. Afshang, and H. S. Dhillon, "Integrated mmWave access and backhaul in 5G: Bandwidth partitioning and downlink analysis," in *Proc. IEEE Int. Conf. Commun. (ICC)*, Jul. 2018, pp. 1–6, doi: 10.1109/ICC.2018.8422149.

[52] C. Saha, M. Afshang, and H. S. Dhillon, "Bandwidth partitioning and downlink analysis in millimeter wave integrated access and backhaul for 5G," *IEEE Trans. Wireless Commun.*, vol. 17, no. 12, pp. 8195–8210, Dec. 2018, doi: 10.1109/TWC.2018.2874655.

[53] Y. Liu, A. Tang, and X. Wang, "Joint incentive and resource allocation design for user provided network under 5G integrated access and backhaul networks," *IEEE Trans. Netw. Sci. Eng.*, vol. 7, no. 2, pp. 673–685, Apr.–Jun. 2020, doi: 10.1109/TNSE.2019.2910867.

[54] G. Kwon and H. Park, "Joint user association and beamforming design for millimeter wave UDN with wireless backhaul," *IEEE J. Sel. Areas Commun.*, vol. 37, no. 12, pp. 2653–2668, Oct. 2019, doi: 10.1109/JSAC.2019.2947926.

[55] A. J. Muhammed, Z. Ma, Z. Zhang, P. Fan, and E. G. Larsson, "Energy-efficient resource allocation for NOMA based small cell networks with wireless backhauls," *IEEE Trans. Commun.*, vol. 68, no. 6, pp. 3766–3781, Jun. 2020, doi: 10.1109/TCOMM.2020.2979971.

[56] W. Lei, Y. Ye, and M. Xiao, "Deep reinforcement learning-based spectrum allocation in integrated access and backhaul networks," *IEEE Trans. Cogn. Commun. Netw.*, vol. 6, no. 3, pp. 970–979, Sep. 2020, doi: 10.1109/TCCN.2020.2992628.

[57] H. Zheng and L. Li, "Joint backhaul bandwidth and power allocation in heterogeneous cellular networks: A two-level approach," *Int. J. Commun. Syst.*, vol. 33, no. 11, p. e4420, Apr. 2020, doi: 10.1002/dac.4420.

[58] M. Pagin, T. Zugno, M. Polese, and M. Zorzi, "Resource management for 5G NR integrated access and backhaul: A semi-centralized approach," *IEEE Trans. Wireless Commun.*, vol. 21, no. 2, pp. 753–767, Feb. 2022, doi: 10.1109/TWC.2021.3098967.

[59] S. Gopalam, S. V. Hanly, and P. Whiting, "Distributed and local scheduling algorithms for mmWave integrated access and backhaul," *IEEE/ACM Trans. Netw.*, vol. 30, no. 4, pp. 1749–1764, Aug. 2022, doi: 10.1109/TNET.2022.3154367.

[60] O. P. Adare, H. Babbili, C. Madapatha, B. Makki, and T. Svensson, "Uplink power control in integrated access and backhaul networks," Oct. 2021, *arXiv:2110.07704*.

[61] E. Chen, M. Tao, and N. Zhang, "User-centric joint access-backhaul design for full-duplex self-backhauled wireless networks," *IEEE Trans. Commun.*, vol. 67, no. 11, pp. 7980–7993, Nov. 2019, doi: 10.1109/TCOMM.2019.2932987.

[62] Y. Xue, X. Zheng, and V. K. N. Lau, "Line-of-sight MIMO for high capacity millimeter wave backhaul in FDD systems," *J. Commun. Inf. Netw.*, vol. 5, no. 2, pp. 177–193, Jun. 2020, doi: 10.23919/JCIN.2020.9130434.

[63] Y. Sadovaya et al., "Self-interference assessment and mitigation in 3GPP IAB deployments," in *Proc. IEEE Int. Conf. Commun. (ICC)*, Aug. 2021, pp. 1–6, doi: 10.1109/ICC42927.2021.9500769.

[64] J. Zhang, H. Luo, N. Garg, M. Holm, and T. Ratnarajah, "Design and analysis of mmWave full-duplex integrated access and backhaul networks," in *Proc. IEEE Int. Conf. Commun. (ICC)*, Jun. 2021, pp. 1–6, doi: 10.1109/ICC42927.2021.9500615.

[65] "Mobile relay for E-UTRA," 3rd Gener. Partnership Project (3GPP), Sophia Antipolis, France, Rep. TR 36.836, Oct. 2012. [Online]. Available: http://www.3gpp.org/ftp/Specs/html-info/36836.htm

[66] "Study on vehicle-mounted relays; stage 1 (release 18), v.18.0.0," 3rd Gener. Partnership Project (3GPP), Sophia Antipolis, France, Rep. TR 22.839, Sep. 2021. [Online]. Available: http://www.3gpp.org/ftp/Specs/html-info/22839.htm

[67] H. Guo, B. Makki, D.-T. Phan-Huy, E. Dahlman, M.-S. Alouini, and T. Svensson, "Predictor antenna: A technique to boost the performance of moving relays," *IEEE Commun. Mag.*, vol. 59, no. 7, pp. 80–86, Jul. 2021, doi: 10.1109/MCOM.001.2001205.

[68] H. Guo, B. Makki, M.-S. Alouini, and T. Svensson, "On delay-limited average rate of HARQ-based predictor antenna systems," *IEEE Wireless Commun. Lett.*, vol. 10, no. 8, pp. 1628–1632, Aug. 2021, doi: 10.1109/LWC.2021.3075351.

[69] H. Guo, B. Makki, M.-S. Alouini, and T. Svensson, "High-rate uninterrupted Internet-of-Vehicle communications in highways: Dynamic blockage avoidance and CSIT acquisition," Sep. 2021, *arXiv:2109.12878*.

[70] D.-T. Phan-Huy, S. Wesemann, J. Bjorsell, and M. Sternad, "Adaptive massive MIMO for fast moving connected vehicles: It will work with predictor antennas!" in *Proc. 22nd Int. ITG Workshop Smart Antennas*, Mar. 2018, pp. 1–8.

[71] Y. Sui, A. Papadogiannis, W. Yang, and T. Svensson, "Performance comparison of fixed and moving relays under co-channel interference," in *Proc. IEEE Global Telecommun. Conf. Workshops (GLOBECOM Workshops)*, Anaheim, CA, USA, Dec. 2012, pp. 574–579, doi: 10.1109/GLOCOMW.2012.6477637.

[72] Y. Sui, A. Papadogiannis, and T. Svensson, "The potential of moving relays—A performance analysis," in *Proc. IEEE Veh. Technol. Conf. (VTC)*, Yokohama, Japan, Jul. 2012, pp. 1–5, doi: 10.1109/VETECS.2012.6240247.

[73] J. Gui and X. Dai, "Stabilizing mmWave backhaul energy efficiency for vehicle-mounted access points by Q-learning-based scheme," *Wireless Pers. Commun.*, vol. 121, pp. 2885–2909, Aug. 2021, doi: 10.1007/s11277-021-08854-w.

[74] Y. Sui, A. Papadogiannis, W. Yang, and T. Svensson, "The energy efficiency potential of moving and fixed relays for vehicular users," in *Proc. IEEE Veh. Technol. Conf. (VTC)*, Las Vegas, NV, USA, Sep. 2013, pp. 1–7, doi: 10.1109/VTCFall.2013.6692436.

[75] S. Jangsher and V. O. K. Li, "Backhaul resource allocation for existing and newly arrived moving small cells," *IEEE Trans. Veh. Technol.*, vol. 66, no. 4, pp. 3211–3219, Apr. 2017, doi: 10.1109/TVT.2016.2590502.

[76] A. Jaziri, R. Nasri, and T. Chahed, "Offloading traffic hotspots using moving small cells," in *Proc. IEEE Int. Conf. Commun. (ICC)*, Kuala Lumpur, Malaysia, May 2016, pp. 1–6, doi: 10.1109/ICC.2016.7511566.

[77] S. Jaffry, S. F. Hasan, and X. Gui, "Efficient resource-sharing algorithms for mobile-cell's sidehaul and access links," *IEEE Netw. Lett.*, vol. 1, no. 2, pp. 72–75, Jun. 2019, doi: 10.1109/LNET.2019.2899870.

[78] S. Jaffry, S. F. Hasan, and X. Gui, "Interference management and resource sharing in moving networks," *IET Commun.*, vol. 13, no. 16, pp. 2580–2589, Oct. 2019, doi: 10.1049/iet-com.2018.6193.

[79] J. Wu and P. Fan, "A survey on high mobility wireless communications: Challenges, opportunities and solutions," *IEEE Access*, vol. 4, pp. 450–476, 2016, doi: 10.1109/ACCESS.2016.2518085.

[80] M. Choi, B. Yoon, D. Kim, and D. Sung, "IAB-based railway communication method for stable service provision," in *Proc. Int. Conf. Ubiquitous Future Netw. (ICUFN)*, Jeju Island, South Korea, Aug. 2021, pp. 176–178, doi: 10.1109/ICUFN49451.2021.9528777.

[81] A. Gonzalez-Plaza et al., "5G communications in high speed and metropolitan railways," in *Proc. Eur. Conf. Antennas Propag.*, Paris, France, Mar. 2017, pp. 658–660, doi: 10.23919/EuCAP.2017.7928756.

[82] B. Ai, A. F. Molisch, M. Rupp, and Z.-D. Zhong, "5G key technologies for smart railways," *Proc. IEEE*, vol. 108, no. 6, pp. 856–893, Jun. 2020, doi: 10.1109/JPROC.2020.2988595.

[83] P. T. Dat, A. Kanno, K. Inagaki, F. Rottenberg, N. Yamamoto, and T. Kawanishi, "High-speed and uninterrupted communication for high-speed trains by ultrafast WDM fiber–wireless backhaul system," *J. Lightw. Technol.*, vol. 37, no. 1, pp. 205–217, Jan. 1, 2019, doi: 10.1109/JLT.2018.2885548.

[84] M. Ichinose and I. Nakagawa, "Verification trials of 5G communications in high-speed mobile environments," *New Breeze*, vol. 30, no. 4, pp. 6–8, Oct. 2018.

[85] J. Xu and B. Ai, "Artificial intelligence empowered power allocation for smart railway," *IEEE Commun. Mag.*, vol. 59, no. 2, pp. 28–33, Feb. 2021, doi: 10.1109/MCOM.001.2000634.

[86] Y. Lu, K. Xiong, P. Fan, Z. Zhong, and B. Ai, "The effect of power adjustment on handover in high-speed railway communication networks," *IEEE Access*, vol. 5, pp. 26237–26250, 2017, doi: 10.1109/ACCESS.2017.2775044.

[87] M. Gao et al., "Efficient hybrid beamforming with anti-blockage design for high-speed railway communications," *IEEE Trans. Veh. Technol.*, vol. 69, no. 9, pp. 9643–9655, Sep. 2020, doi: 10.1109/TVT.2020.3000757.

[88] S. Jangsher and V. O. K. Li, "Resource allocation in cellular networks with moving small cells with probabilistic mobility," in *Proc. IEEE Pers. Indoor Mobile Radio Commun. (PIMRC)*, Washington, DC, USA, Jun. 2014, pp. 1701–1705, doi: 10.1109/PIMRC.2014.7136442.

[89] S. Chae, M. Z. Chowdhury, T. Nguyen, and Y. M. Jang, "A dynamic frequency allocation scheme for moving small-cell networks," in *Proc. Int. Conf. ICT Converg. (ICTC)*, Jeju Island, South Korea, Dec. 2012, pp. 125–128, doi: 10.1109/ICTC.2012.6386795.

[90] A. Mastrosimone and D. Panno, "New challenge: Moving network based on mmWave technology for 5G era," in *Proc. Int. Conf. Comput. Inf. Telecommun. Syst. (CITS)*, Gijon, Spain, Oct. 2015, pp. 1–5, doi: 10.1109/CITS.2015.7297756.

[91] A. Mastrosimone and D. Panno, "A comparative analysis of mmWave vs LTE technology for 5G moving networks," in *Proc. IEEE Wireless Mobile Comput. Netw. Commun. (WiMob)*, Abu Dhabi, UAE, Dec. 2015, pp. 422–429, doi: 10.1109/WiMOB.2015.7347993.

[92] A. Mastrosimone and D. Panno, "Moving network based on mmWave technology: A promising solution for 5G vehicular users," *Wireless Netw.*, vol. 24, no. 7, pp. 2409–2426, Mar. 2017, doi: 10.1007/s11276-017-1479-0.

[93] S. Jaffry, S. F. Hasan, and X. Gui, "Shared spectrum for mobile-cell's backhaul and access link," in *Proc. IEEE Global Telecommun. Conf. (GLOBECOM)*, Abu Dhabi, UAE, Dec. 2018, pp. 1–6, doi: 10.1109/GLOCOM.2018.8647131.

[94] S. Jaffry, S. F. Hasan, and X. Gui, "Effective resource sharing in mobile-cell environments," Aug. 2018, *arXiv:1808.01700*.

[95] M. Tayyab, G. P. Koudouridis, X. Gelabert, and R. Jäntti, "Handover performance and power consumption analysis of lte mobile relays," in *Proc. IEEE Veh. Technol. Conf. (VTC)*, Victoria, BC, Canada, Nov. 2020, pp. 1–5, doi: 10.1109/VTC2020-Fall49728.2020.9348720.

[96] R. Raheem, A. Lasebae, and J. Loo, "Performance evaluation of LTE network via using fixed/mobile femtocells," in *Proc. Int. Conf. Adv. Inf. Netw. Appl. Workshops*, Victoria, BC, Canada, May 2014, pp. 255–260, doi: 10.1109/WAINA.2014.51.

[97] M. Z. Chowdhury, S. H. Chae, and Y. M. Jang, "Group handover management in mobile femtocellular network deployment," in *Proc. Int. Conf. Ubiquitous Future Netw. (ICUFN)*, Phuket, Thailand, Aug. 2012, pp. 162–165, doi: 10.1109/ICUFN.2012.6261685.

[98] I. Bor-Yaliniz, M. Salem, G. Senerath, and H. Yanikomeroglu, "Is 5G ready for drones: A look into contemporary and prospective wireless networks from a standardization perspective," *IEEE Wireless Commun.*, vol. 26, no. 1, pp. 18–27, Feb. 2019, doi: 10.1109/MWC.2018.1800229.

[99] M. Gapeyenko, V. Petrov, D. Moltchanov, S. Andreev, N. Himayat, and Y. Koucheryavy, "Flexible and reliable UAV-assisted backhaul operation in 5G mmWave cellular networks," *IEEE J. Sel. Areas Commun.*, vol. 36, no. 11, pp. 2486–2496, Nov. 2018, doi: 10.1109/JSAC.2018.2874145.

[100] A. A. Khuwaja, Y. Zhu, G. Zheng, Y. Chen, and W. Liu, "Performance analysis of hybrid UAV networks for probabilistic content caching," *IEEE Syst. J.*, vol. 15, no. 3, pp. 4013–4024, Sep. 2021, doi: 10.1109/JSYST.2020.3013786.

[101] N. Tafintsev et al., "Aerial access and backhaul in mmWave B5G systems: Performance dynamics and optimization," *IEEE Commun. Mag.*, vol. 58, no. 2, pp. 93–99, Feb. 2020, doi: 10.1109/MCOM.001.1900318.

[102] A. Perez, A. Fouda, and A. S. Ibrahim, "Ray tracing analysis for UAV-assisted integrated access and backhaul millimeter wave networks," in *Proc. IEEE Int. Symp. World Wireless Mobile Multimedia Netw. (WoWMoM)*, Washington, DC, USA, Aug. 2019, pp. 1–5, doi: 10.1109/WoWMoM.2019.8792969.

[103] E. Kalantari, M. Z. Shakir, H. Yanikomeroglu, and A. Yongacoglu, "Backhaul-aware robust 3D drone placement in 5G+ wireless networks," in *Proc. IEEE Int. Conf. Commun. Workshops (ICC Workshops)*, Paris, France, Jul. 2017, pp. 109–114, doi: 10.1109/ICCW.2017.7962642.

[104] A. Fouda, A. S. Ibrahim, I. Guvenc, and M. Ghosh, "UAV-based in-band integrated access and backhaul for 5G communications," in *Proc. IEEE Veh. Technol. Conf. (VTC)*, Chicago, IL, USA, Apr. 2018, pp. 1–5, doi: 10.1109/VTCFall.2018.8690860.

[105] A. Fouda, A. S. Ibrahim, İ. Güvenç, and M. Ghosh, "Interference management in UAV-assisted integrated access and backhaul cellular networks," *IEEE Access*, vol. 7, pp. 104553–104566, 2019, doi: 10.1109/ACCESS.2019.2927176.

[106] C. Qiu, Z. Wei, Z. Feng, and P. Zhang, "Joint resource allocation, placement and user association of multiple UAV-mounted base stations with in-band wireless backhaul," *IEEE Wireless Commun. Lett.*, vol. 8, no. 6, pp. 1575–1578, Dec. 2019, doi: 10.1109/LWC.2019.2928544.

[107] E. Kalantari, I. Bor-Yaliniz, A. Yongacoglu, and H. Yanikomeroglu, "User association and bandwidth allocation for terrestrial and aerial base stations with backhaul considerations," in *Proc. IEEE Pers. Indoor Mobile Radio Commun. (PIMRC)*, Montreal, QC, Canada, Oct. 2017, pp. 1–6, doi: 10.1109/PIMRC.2017.8292783.

[108] H. Zhang and L. Dai, "Mobility prediction: A survey on state-of-the-art schemes and future applications," *IEEE Access*, vol. 7, pp. 802–822, 2019, doi: 10.1109/ACCESS.2018.2885821.

[109] L. Zhang and N. Ansari, "A framework for 5G networks with in-band full-duplex enabled drone-mounted base-stations," *IEEE Wireless Commun.*, vol. 26, no. 5, pp. 121–127, Oct. 2019, doi: 10.1109/MWC.2019.1800486.

[110] L. Zhang and N. Ansari, "Backhaul-aware uplink communications in full-duplex DBS-aided HetNets," in *Proc. IEEE Global Telecommun. Conf. (GLOBECOM)*, Waikoloa, HI, USA, Dec. 2019, pp. 1–6, doi: 10.1109/GLOBECOM38437.2019.9013471.

[111] J. Liu, Y. Shi, Z. M. Fadlullah, and N. Kato, "Space–air–ground integrated network: A survey," *IEEE Commun. Surveys Tuts.*, vol. 20, no. 4, pp. 2714–2741, 4th Quart., 2018, doi: 10.1109/COMST.2018.2841996.

[112] J. Sheng et al., "Space–air–ground integrated network development and applications in high-speed railways: A survey," *IEEE Trans. Intell. Transp. Syst.*, vol. 23, no. 8, pp. 10066–10085, Aug. 2022, doi: 10.1109/TITS.2021.3118557.

[113] M. M. Azari et al., "Evolution of non-terrestrial networks from 5G to 6G: A survey," *IEEE Commun. Surveys Tuts.*, vol. 24, no. 4, pp. 2633–2672, 4th Quart., 2022, doi: 10.1109/COMST.2022.3199901.

[114] Y. Hu, M. Chen, and W. Saad, "Joint access and backhaul resource management in satellite-drone networks: A competitive market approach," *IEEE Trans. Wireless Commun.*, vol. 19, no. 6, pp. 3908–3923, Jun. 2020, doi: 10.1109/TWC.2020.2979127.

[115] M. Liu, G. Feng, L. Cheng, and S. Qin, "A deep reinforcement learning based adaptive transmission strategy in space–air–ground integrated networks," in *Proc. IEEE Int. Conf. Commun. (ICC)*, 2022, pp. 4697–4702, doi: 10.1109/ICC45855.2022.9838681.

[116] R. Deng, B. Di, S. Chen, S. Sun, and L. Song, "Ultra-dense LEO satellite offloading for terrestrial networks: How much to pay the satellite operator?" *IEEE Trans. Wireless Commun.*, vol. 19, no. 10, pp. 6240–6254, Oct. 2020, doi: 10.1109/TWC.2020.3001594.

[117] R. Samy, H.-C. Yang, T. Rakia, and M.-S. Alouini, "Space–air–ground FSO networks for high-throughput satellite communications," *IEEE Commun. Mag.*, early access, Sep. 12, 2022, doi: 10.1109/MCOM.002.2200018.

[118] C. Han, L. Bai, T. Bai, and J. Choi, "Joint UAV deployment and power allocation for secure space–air–ground communications," *IEEE Trans. Commun.*, vol. 70, no. 10, pp. 6804–6818, Oct. 2022, doi: 10.1109/TCOMM.2022.3203471.

[119] F. Tang, C. Wen, M. Zhao, and N. Kato, "Machine learning for space–air–ground integrated network assisted vehicular network: A novel network architecture for vehicles," *IEEE Veh. Technol. Mag.*, vol. 17, no. 3, pp. 34–44, Sep. 2022, doi: 10.1109/MVT.2022.3188405.

[120] H. Li, K. Ota, and M. Dong, "AI in SAGIN: Building deep learning service-oriented space–air–ground integrated networks," *IEEE Netw.*, early access, Aug. 1, 2022, doi: 10.1109/MNET.001.2000512.

[121] P. Agyapong et al., "Simulation guidelines," METIS, Stockholm, Sweden, document ICT-317669-METIS/D6.1, Oct. 2013. Accessed: Sep. 20, 2021. [Online]. Available: https://metis2020.com/wp-content/uploads/deliverables/METIS_D6.1_v1.pdf

[122] Y. Sui, I. Guvenc, and T. Svensson, "Interference management for moving networks in ultra-dense urban scenarios," *EURASIP J. Wireless Commun. Netw.*, vol. 111, pp. 1–32, Apr. 2015, doi: 10.1186/s13638-015-0326-1.

[123] "Study on channel model for frequencies from 0.5 to 100 GHz, v.14.2.0," 3rd Gener. Partnership Project (3GPP), Sophia Antipolis, France, Rep. TR 38.901, Sep. 2017. Accessed: Sep. 26, 2017. [Online]. Available: http://www.3gpp.org/DynaReport/38901.htm

[124] *User Equipment (UE) Radio Transmission and Reception; Part 2: Range 2 Standalone, V.17.6.0*, 3GPP Standard TS 38.101-2, Jun. 2022. [Online]. Available: https://www.3gpp.org/DynaReport/38101-2.htm

[125] A. M. Pessoa et al., "A stochastic channel model with dual mobility for 5G massive networks," *IEEE Access*, vol. 7, pp. 149971–149987, 2019, doi: 10.1109/ACCESS.2019.2947407.

[126] *Evolved Universal Terrestrial Radio Access (E-UTRA); Physical Channels and Modulation, V.16.6.0*, 3GPP Standard TS 36.211, Jun. 2021. [Online]. Available: http://www.3gpp.org/ftp/Specs/html-info/36211.htm

[127] *NR; Physical Layer Measurements*, 3GPP Standard TS 38.215, Sep. 2018. Accessed: Oct. 15, 2018. [Online]. Available: http://www.3gpp.org/ftp/Specs/html-info/38215.htm

[128] *NR; Physical Layer Procedures For Data, V.15.0.0*, 3GPP Standard TS 38.214, Dec. 2017. [Online]. Available: http://www.3gpp.org/ftp/Specs/html-info/38214.htm

[129] *Study on Evaluation Methodology of New Vehicle-to-Everything (V2X) Use Cases for LTE and NR, V.15.2.0*, 3GPP Standard TS 37.885, Dec. 2018. Accessed: Apr. 17, 2019. [Online]. Available: http://www.3gpp.org/ftp/Specs/html-info/37885.htm

[130] V. F. Monteiro et al., "TDD frame design for interference handling in mobile IAB networks," Apr. 2022, *arXiv:2204.13198*.

[131] N. Rajatheva et al., "Scoring the terabit/s goal:Broadband connectivity in 6G," Feb. 2021, *arXiv:2008.07220*.
[132] "IAB enhancements for Rel 17," 3rd Gener. Partnership Project (3GPP), Sophia Antipolis, France, RP 192709, tSG-RAN WG3 meeting no. 86, Dec. 2019. Accessed: Sep. 13, 2021. [Online]. Available: https://www.3gpp.org/ftp/TSG_RAN/TSG_RAN/TSGR_86/Docs/RP-192709.zip
[133] "IAB topology update procedure," 3rd Gener. Partnership Project (3GPP), Sophia Antipolis, France, document R3 212413, tSG-RAN WG3 meeting no. 112-e, May 2021. Accessed: Sep. 13, 2021. [Online]. Available: https://www.3gpp.org/ftp/TSG_RAN/WG3_Iu/TSGR3_112-e/Docs/R3-212413.zip
[134] "Principles of group mobility for inter-donor IAB-node migration," 3rd Gener. Partnership Project (3GPP), Sophia Antipolis, France, document R3 206332, tSG-RAN WG3 meeting no. 110-e, Nov. 2020. Accessed: Sep. 13, 2021. [Online]. Available: https://www.3gpp.org/ftp/TSG_RAN/WG3_Iu/TSGR3_110-e/Docs/R3-206332.zip

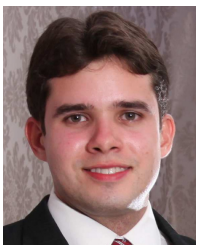

VICTOR F. MONTEIRO received the double B.Sc. degree in general engineering from École Centrale Lyon, France, and in telecommunications engineering *(magna cum laude)* from the Federal University of Ceará (UFC), Fortaleza, Brazil, in 2013, and the M.Sc. and Ph.D. degrees in telecommunications engineering from UFC in 2015 and 2019, respectively, where he is currently a Visiting Professor. Since 2014, he has been a Researcher with the Wireless Telecom Research Group, UFC, where he has worked in projects in cooperation with Ericsson Research, Luleå, Sweden. In 2016, he was an Invited Researcher with Ericsson Research, where he worked for six months on the topic of LTE-NR Dual Connectivity. Besides, in 2017/2018, he spent one year at Ericsson Research, Stockholm, Sweden, where he worked on the topics of mobility management and channel hardening. From 2010 to 2012, he took part, in France, of the Eiffel Excellence Scholarship Program established by the French Ministry of Foreign Affairs. His research interests include 5G architecture and protocols, 5G measurement and reporting procedures, mobility management, and radio resource allocation.

FRANCISCO RAFAEL M. LIMA (Senior Member, IEEE) received the B.Sc. degree (with Hons.) in electrical engineering and the M.Sc. and D.Sc. degrees in telecommunications engineering from the Federal University of Ceará, Fortaleza, Brazil, in 2005, 2008, and 2012, respectively. In 2008, he has been in an internship with Ericsson Research, Luleå, Sweden, where he studied scheduling algorithms for LTE System. Since 2010, he has been a Professor of Computer Engineering Department with the Federal University of Ceará, Sobral, Brazil. He is also a Senior Researcher with the Wireless Telecom Research Group, Fortaleza, Brazil, where he works in projects in cooperation with Ericsson Research. He has published several conference and journal articles as well as patents in the wireless telecommunications field. His research interests include radio resource allocation algorithms for QoS guarantees for 5G and beyond 5G networks in scenarios with multiple services, resources, antennas, and users.

DARLAN C. MOREIRA received the B.Sc. degree in electrical engineering and the M.S. and Ph.D. degrees in teleinformatics engineering from the Federal University of Ceará, Fortaleza, Brazil, in 2005, 2007, and 2020, respectively. In 2007, he was an Invited Researcher with Ericsson Research, Kista, Sweden, where he worked for three months. In 2010, he was an Invited Researcher with Supélec in Gif-sur-Yvette, France, for six months. Since 2005, he has been a Researcher with Wireless Telecommunications Research Group, Brazil, where he has been working in projects within the technical cooperation between GTEL and Ericsson Research. Some topics of his research interests include machine learning, MIMO transceiver design, channel estimation, interference management, integrated access and backhaul, and modeling and simulation of cellular communication.

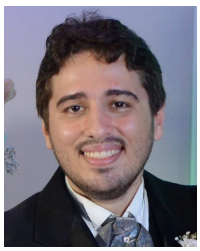

DIEGO A. SOUSA received the B.Sc. degree in computer engineering from the University of Ceará (UFC), Sobral, Brazil, in 2011, and the M.Sc. and Ph.D. degrees in teleinformatics engineering from UFC, Fortaleza, Brazil, in 2013 and 2018, respectively. Since 2013, he has been a Researcher with the Wireless Telecom Research Group, UFC, participating of projects in a technical and scientific cooperation with Ericsson Research. Also, since 2013, he has been a Professor with the Federal Institute of Education, Science, and Technology of Ceará, Paracuru, Brazil. His research interests include numerical optimization, 5G networks, coordinated scheduling, and radio resource management for QoS/QoE provisioning.

TARCISIO F. MACIEL received the B.Sc. and M.Sc. degrees in electrical engineering from the Federal University of Ceará (UFC) in 2002 and 2004, respectively, and the Dr.Ing. degree in electrical engineering from Technische Universitat Darmstat (TUD), Germany, in 2008. Since 2001, he has actively participated in several projects in a technical and scientific cooperation between the Wireless Telecommunications Research Grupo, UFC, and Ericsson Research. From 2005 to 2008, he was a Research Assistant with the Communications Engineering Laboratory, TUD. Since 2008, he has been a member of the Post-Graduation Program in Teleinformatics Engineering, UFC. In 2009, he was a Professor of Computer Engineering with UFC-Sobral and since 2010, he has been a Professor with the Center of Technology, UFC. His research interests include radio resource management, numerical optimization, and multi-user/multi-antenna communications.

BEHROOZ MAKKI (Senior Member, IEEE) received the Ph.D. degree in communication engineering from the University of Technology, Gothenburg, Sweden. He was a Postdoctoral Researcher with the Chalmers University of Technology from 2013 to 2017. He is currently working as a Senior Researcher with Ericsson Research, Gothenburg. He has co-authored 67 journal papers, 47 conference papers, and 90 patent applications. His current research interests include integrated access and backhaul, green communications, millimeter wave communications, NOMA, and backhauling. He is a recipient of the VR Research Link Grant, Sweden, in 2014, the Ericsson's Research Grant, Sweden, in 2013, 2014, and 2015, the ICT SEED Grant, Sweden, in 2017, as well as the Wallenbergs Research Grant, Sweden, in 2018. He is also a recipient of the IEEE Best Reviewer Award for IEEE TRANSACTIONS ON WIRELESS COMMUNICATIONS in 2018 and the IEEE Best Editor Award for IEEE WIRELESS COMMUNICATIONS LETTERS in 2020. He is currently working as an Editor for IEEE TRANSACTIONS ON COMMUNICATIONS, IEEE WIRELESS COMMUNICATIONS LETTERS, and IEEE COMMUNICATIONS LETTERS. He was a member of the European Commission Projects "mm-Wave Based Mobile Radio Access Network for 5G Integrated Communications" and "ARTIST4" as well as various national and international research collaborations.

HANS HANNU received the M.Sc. degree in electrical engineering/signal processing from the Luleå University of Technology, 1998, Sweden. He has been a Master Research Engineer with Ericsson Research since 2011. He works in areas as service realization and performance over cellular networks, including radio access and network transport protocol, with algorithm development, such as data transmission scheduling, and project management. He has co-authored 47 granted patents.